

On the Effects of Resolution Inhomogeneity in LES

Gopal R. Yalla¹, Todd A. Oliver¹, Sigfried W. Haering^{1,2}, Björn Engquist^{1,3}, and Robert D. Moser^{1,4}

¹The Oden Institute for Computational Engineering and Sciences, The University of Texas at Austin

²Argonne National Laboratories

³Department of Mathematics, The University of Texas at Austin

⁴Department of Mechanical Engineering, The University of Texas at Austin

July 20, 2022

Abstract

Large Eddy Simulation (LES) of turbulence in complex geometries is often conducted using discretizations with highly inhomogeneous resolution. The issues associated with resolution inhomogeneity are related to the noncommutativity of the filtering and differentiation operators, often referred to as the commutation error. While the commutation error is well recognized, it is often ignored in practice. Moreover, the commutation error related to the implicit filter (i.e., projection onto the underlying discretization) has not been well investigated. Most of the previous work concerning the commutation error has only applied to smooth convolution filters or has only addressed the additional commutation error that arises from applying explicit filters on top of the implicit filter. Modeling of the implicit commutation error that arises from the noncommutativity between numerical projection and differentiation is crucial for correcting errors induced by resolution inhomogeneity that arise in practical LES settings. Here, we investigate how the implicit commutation error manifests in simulation and demonstrate its impact on the convection of a packet of homogeneous isotropic turbulence through an inhomogeneous grid. A connection is made between the implicit commutation error and the propagation properties of the underlying numerics. A model is proposed for the correction of these issues in the case considered here, which highlights important characteristics of commutation models for LES and the importance of considering numerical properties during the formulation of subgrid stress models in general. Several insights are discussed that could also be applied to other issues in LES, such as discretization error.

1 Introduction

Computational simulation of fluid flow plays an increasingly important role in understanding the physics that govern many complex engineering systems. However, the utility of simulation is limited by the reliability of the underlying models and numerical methods. This is particularly problematic in turbulence modeling where challenging flow features, a wide range of interacting scales, limited computational resources, and complex geometries combine to demand highly sophisticated models. Large Eddy Simulation (LES) has long been promised to be a computationally tractable solution to many of the challenges associated with the simulation of practical turbulent flows. However, several deficiencies of LES must still be addressed before this promise is fulfilled. In particular, LES models are typically built with the assumption of isotropic unresolved turbulence in equilibrium with the large scales, homogeneous isotropic filtering/resolution, and proper representation of all resolved scales by the underlying numerics. All of these assumptions are violated in practical simulations of high Reynolds number flows. In this work, we address the issue of inhomogeneous filtering/resolution.

The issues associated with resolution inhomogeneity are related to the noncommutativity of the filtering and differentiation operators in the filtered Navier-Stokes equations. This is referred to as commutation error, first introduced by Ghosal and Moin [1]. Since then, several investigators have acknowledged the significant impact commutation error can have on the solution [2, 3, 4, 5, 6, 7, 8, 9, 10, 11]. Despite this, correction of the commutation error is often ignored in practice because of the modeling challenges involved. Nevertheless, correction of the commutation error is crucial for developing robust subgrid stress (SGS) models for practical LES applications. Furthermore, Hamba [12] showed that the impact of resolution inhomogeneity on hybrid RANS/LES applications can be significant because the resolution must change drastically when transitioning to/from LES and RANS regions. Modeling of commutation effects will, therefore, also be necessary for these more sophisticated turbulence modeling techniques, which inherit the deficiencies of the traditional SGS models they are based upon.

Most of the previous work addressing the commutation error has come out of the explicit filtering community. Motivated by controlling numerical error arising from inadequately resolved scales of motion, the explicit filtering approach attempts to “separate” the filter from the discretization by defining an explicit filter whose width is much larger than the mesh spacing [10, 13, 14, 15, 16, 17]. Commutativity with differentiation is viewed as a requirement of explicit filters to address the commutation error. In this context, van der Ven [2] introduced a one-parameter family of analytical filters that commute with differentiation up to a given order in filter width. Vasilyev et al. [3] generalized the work of [1] and developed a set of constraints for constructing discrete filters that commute with differentiation up to a desired order. This work was extended to unstructured meshes by Marsden et al. [4].

Projection onto the discretization is ultimately responsible for discarding information of the turbulent field, so the discretization cannot be separated from the filter since it *is* the filter (often referred to as an implicit filter.) Therefore, commutative explicit filters only ensure that the explicit filtering process does not introduce any commutation error *in addition* to that introduced by the implicit filter. While this is certainly a necessary requirement for the explicit filtering approach, it does not address the main issues of the commutation error that arise in practical LES settings. It should also be noted that most LES applications rely solely on implicit filtering. Similarly, the original analysis of Ghosal and Moin [1] only applies to smooth convolution filters, not implicit filters. The *implicit commutation error* arising from the noncommutativity between numerical projection and differentiation has not been well investigated and is the focus of this work.

In this paper, we investigate how the implicit commutation error manifests in simulation. We uncover the requirements of SGS models in regions of resolution inhomogeneity by examining the impact of the implicit commutation error on a turbulent field as it convects through an inhomogeneous grid. This study enables the development of new models that are able to correct for the deficiencies of traditional SGS models in these contexts. These findings are crucial for the development of robust turbulence models for practical LES applications, which often depend heavily on the use inhomogeneous grids.

The remainder of this paper is organized as follows: the implicit commutation error is investigated in Section 2; existing literature on numerical wave propagation is reviewed in the context of the commutation error in Section 2.1, and the impact of the implicit commutation error on the convection of a packet of homogeneous isotropic turbulence is demonstrated in Section 2.2. A commutation model is then developed in Section 3; several aspects of its formulation are discussed in Section 3.1, and its ability to correct for the

commutation error is demonstrated in Section 3.2. A conclusion is presented in Section 4.

2 Implicit Commutation Error

As in [1], it is useful to examine the effects of the commutation error on the filtered one-dimensional advection equation:

$$\overline{\frac{\partial u}{\partial t} + a \frac{\partial u}{\partial x}} = 0, \quad (1)$$

where a is the convection velocity. Here, $\overline{(\cdot)}$ denotes the implicit filter which includes a projection onto the underlying discretization that maps an infinite dimensional field to a finite dimensional space. Furthermore, let $\delta/\delta x$ denote a discrete derivative operator. Together, the implicit filter and the discrete derivative operators define what scales are represented by the resolved field. Equation (1) can be written as

$$\frac{\partial \bar{u}}{\partial t} + a \frac{\delta \bar{u}}{\delta x} = -a \mathcal{C}(u), \quad (2)$$

where $\mathcal{C}(u) = \overline{\partial u / \partial x} - \delta \bar{u} / \delta x$. The commutator $\mathcal{C}(u)$ can be decomposed into an inhomogeneous and homogeneous part as $\mathcal{C}(u) = \mathcal{C}^I(u) + \mathcal{C}^H(u)$ where,

$$\mathcal{C}^I(u) = \frac{\overline{\partial u}}{\partial x} - \frac{\overline{\partial u}}{\partial \xi} \frac{\partial \xi}{\partial x}, \quad \mathcal{C}^H(u) = \frac{\overline{\partial u}}{\partial \xi} \frac{\partial \xi}{\partial x} - \frac{\delta \bar{u}}{\delta x}, \quad (3)$$

and ξ is a new spatial coordinate in which the grid is uniform as in [1]. This formulation can be extended to three dimensions as well as to the full Navier-Stokes equations.

Equation (2) makes it clear that a model is needed for both \mathcal{C}^I and \mathcal{C}^H . However, directly modeling these terms is difficult in practice. For example, a model for \mathcal{C}^H must correct for the difference between exact and numerical differentiation. It is common to ignore these terms, which results in commutation error (ignoring \mathcal{C}^I) and discretization error (ignoring \mathcal{C}^H). Another modeling approach which is to develop models that mitigates each of these errors after the fact. For example, approaches for mitigating errors introduced by the absence of \mathcal{C}^H includes explicit filtering (as mentioned previously) and hyperviscosity filters [18]. Neither the effect nor the modeling of the commutation error as related to the implicit filter has been well investigated. Therefore, we are particularly focused on the term \mathcal{C}^I in this paper, although several insights related to \mathcal{C}^H are made because of their inherent connection through \mathcal{C} .

When convecting through coarsening grids, the resolved turbulence in a fine region of the grid will be moving into a coarse region of the grid in which all the resolved scales can no longer be represented. If (1) could be solved directly, or if \mathcal{C}^I could be modeled exactly, the governing equations would ensure that the amount of resolved energy always corresponds with the local grid spacing by transferring the appropriate amount of energy in the resolved scales to the subgrid scales. In other words, the commutation error is responsible for resolved turbulence reaching a state of unresolvability on the grid. A commutation model for \mathcal{C}^I must provide the correct transfer rate to the subgrid scales as the resolved turbulence flows through coarsening grid regions.

Similarly, a commutation model must provide the appropriate production of resolved turbulent kinetic energy as the turbulence convects through refining grids. However, in the refining grid case, there is no particular consistency issue as the coarsely resolved turbulence will be well represented in the fine resolution region. Nevertheless, it is desirable for the resolved turbulence to populate all the scales that can be supported in the fine region. This requires an active forcing formulation dependent on the newly available length scales of the underlying discretization. Notice that the requirements of the commutation model in the coarsening grid case are vastly different than in the refining grid case. It is expressed in the literature that a “good” commutation model should handle both of these scenarios [8], however, we argue that because of these vastly different requirements, a commutation model for the coarsening and refining grid cases should be developed independently. We are particularly focused on flow through coarsening grids in this paper because of the inherent consistency issue. Forcing through refining grids will be the focus of future work.

To further our understanding of what is required of SGS models in regions of resolution inhomogeneity as well as the impact the commutation error can have on LES, it will be important to understand how the implicit commutation error manifests in simulation. We will need to understand the numerical consequence of having resolved turbulence flow into the region of the grid in which it can no longer be resolved. Moreover,

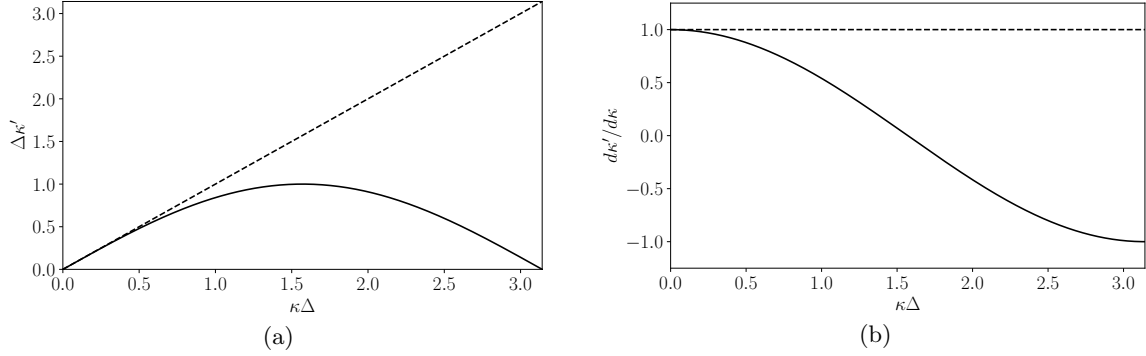


Figure 1: The (a) dispersion relation and (b) group velocity for second-order centered difference numerics compared with the exact form given by spectral numerics; — (Centered Difference), - - - (Spectral).

as in the case of \mathcal{C}^H mentioned above, it may be more feasible to develop a commutation model that mitigates the commutation error, opposed to modeling \mathcal{C}^I directly. Exploration of these two modeling approaches will also rely on our understanding of how the commutation error manifests. In the following section we provide a brief review of numerical wave propagation in the context of the commutation error as this will be crucial for understanding the issues of resolution inhomogeneity.

2.1 Numerical Wave Propagation

Ignoring the commutator \mathcal{C} in (2) gives:

$$\frac{\partial \bar{u}}{\partial t} + a \frac{\delta \bar{u}}{\delta x} = 0, \quad (4)$$

which is what is typically done in LES. We are interested in evolving (4) through an inhomogeneous grid to demonstrate how the commutation error affects the propagation of a wave packet. The wave packet is taken to be initially well resolved by the numerics so there is no contribution from poorly represented scales, i.e., $\mathcal{C}^H \approx 0$, and we are just focused on the absence of \mathcal{C}^I . Consider the implicit filter defined by a Fourier cutoff filter followed by discrete sampling onto the grid and the numerical derivatives defined by a second-order centered difference scheme. Let Δ be the grid spacing/filter width. For uniform Δ , (4) becomes

$$\frac{\partial u_j}{\partial t} = -a \left(\frac{u_{j+1} - u_{j-1}}{2\Delta} \right). \quad (5)$$

It is well recognized that sinusoidal waves of a given frequency ω propagate through discrete grids at a phase velocity that depends on their wavenumber κ [19]. The relation $\omega = \omega(\kappa)$ is called the *dispersion relation*. Individual waves propagate at a phase speed given by $c(\kappa) = \omega(\kappa)/\kappa$; however, the evolution of a packet of a single or multiple wavenumber(s) (as is relevant in the case of LES) is governed by the *group velocity*:

$$\mathcal{G}(\kappa) = \frac{d\omega}{d\kappa}(\kappa). \quad (6)$$

The group velocity is the velocity at which energy is propagated through a discrete grid. Inserting the form $u_j = e^{i(\kappa x_j - \omega t)}$ into (5) yields the dispersion relation $\omega(\kappa) = a\kappa'$, where

$$\kappa' = \frac{\sin(\kappa\Delta)}{\Delta}, \quad (7)$$

is the spectrum of second-order centered difference first derivative operator and is often referred to as the *effective* (or *modified*) wavenumber. Since the only discrete operator in (5) is the first spatial derivative, the dispersion relation is determined by the effective wavenumber. Applying (6) to (7) gives the group velocity for the second-order centered difference scheme:

$$\mathcal{G}(\kappa) = a \cos(\kappa\Delta). \quad (8)$$

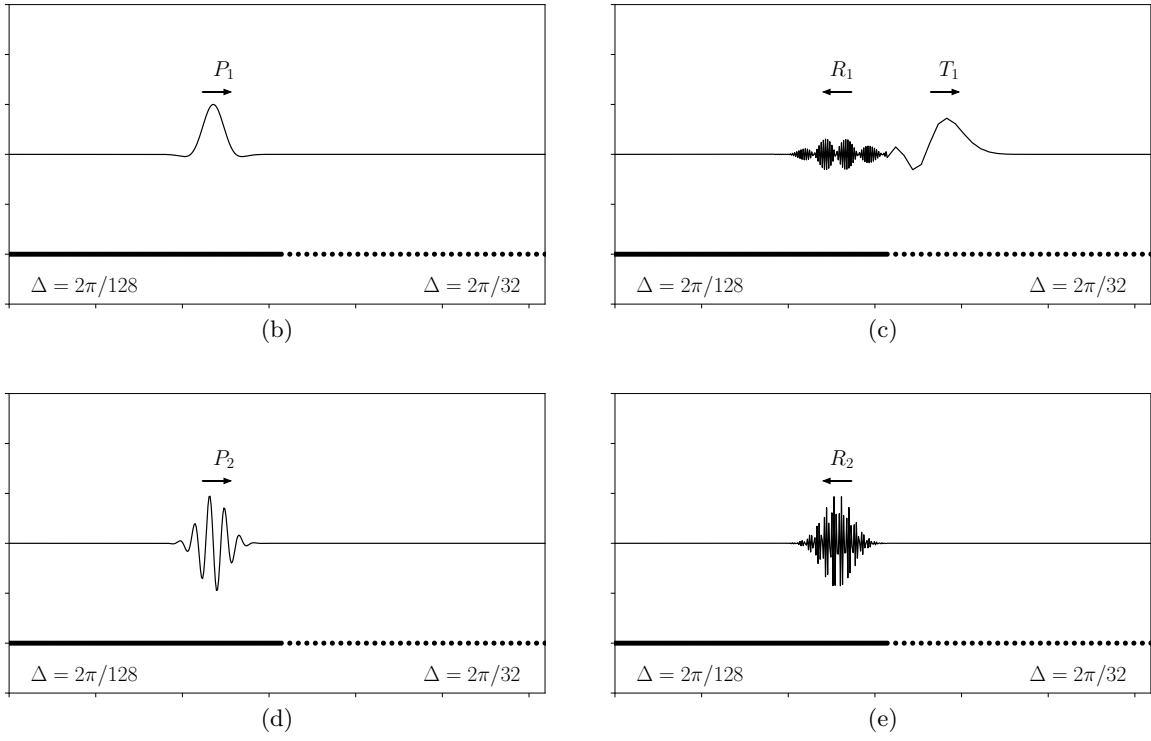
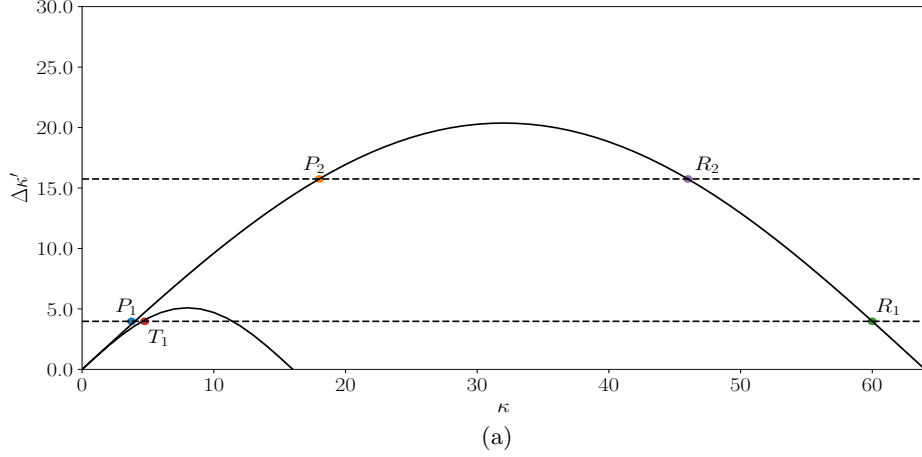


Figure 2: (a) The second order centered difference dispersion relation for both the fine ($\Delta = 2\pi/128$) and coarse ($\Delta = 2\pi/32$) regions of the grid. (b) An incident wave P_1 (•) that can be resolved in both the fine and coarse regions. (c) The subsequent reflected wave R_1 (•) and transmitted wave T_1 (•) after the P_1 wave has propagated through the resolution change. (d) An incident wave P_2 (•) that can only be resolved in the fine region. (e) The subsequent reflected wave R_2 (•) after the P_2 wave has propagated through the resolution change.

Plots of $\omega(\kappa)$ and $\mathcal{G}(\kappa)$ are shown in Figure 1. Let $\kappa_c = \pi/\Delta$ denote the cutoff wavenumber corresponding to the Nyquist wavenumber for the grid as in a LES, and κ_a denote the apex wavenumber at which the group velocity vanishes, i.e., $0 < \kappa < \kappa_a$ has positive group velocity and $\kappa_a < \kappa < \kappa_c$ has negative group velocity. For second-order centered difference schemes $(\kappa_a \Delta) = \pi/2$. Vichnevetsky [20] showed numerical solutions of (5) can be expressed as the superposition of two fundamental types of solutions, $u_j(t) = p_j(t) + q_j(t)$, where solutions of type p propagate *forward* with positive group velocity and correspond to spatial wavenumbers $\kappa \Delta \leq \kappa_a \Delta$, and solutions of type q propagate *backward* with the negative group velocity and correspond to spatial wavenumbers $\kappa \Delta \geq \kappa_a \Delta$. The existence of the two solutions stems from the fact that there are

two available wavenumbers per frequency, as is evident in Figure 1a. Solutions of type p are a consistent approximation of the genuine solution to the advection equation, while solutions of type q are entirely spurious.

Figure 2 shows the result of convecting a wave packet through a sharp change in grid resolution using (5). In Figures 2b and 2c, the initial condition (which we refer to as P_1) is taken to be a wave packet that can be represented in both the fine and coarse regions of the grid. In contrast, in Figures 2d and 2e, the initial wave packet (P_2) can only be resolved in the fine region of the grid. On a uniform grid, no energy is exchanged between solutions of type p and type q , but this is not the case on an inhomogeneous grid. As the incident wave P_1 reaches the interface between the fine and coarse regions, not only is a wave (T_1) of type p transmitted through the interface, but also a reflected wave (R_1) of type q is generated that travels backward with negative group velocity. Since (5) is an energy preserving approximation of (4), the energy from the incident wave is split between the reflected wave and the transmitted wave [20, 21, 22, 23]. Vichnevetsky [22] and Long and Thuburn [23] showed the *reflection ratio*,

$$\frac{\mathcal{R}}{\mathcal{P}} = \frac{G_{\mathcal{P}} - G_{\mathcal{T}}}{G_{\mathcal{T}} + G_{\mathcal{P}}} = \frac{\sqrt{1 - \left(\frac{\omega\Delta}{c}\right)^2} - \sqrt{1 - \left(\frac{\omega\gamma\Delta}{c}\right)^2}}{\sqrt{1 - \left(\frac{\omega\Delta}{c}\right)^2} + \sqrt{1 - \left(\frac{\omega\gamma\Delta}{c}\right)^2}}, \quad (9)$$

captures the amount of reflected energy at the interface, where $\mathcal{G}_{\mathcal{P}}, \mathcal{G}_{\mathcal{T}}, \mathcal{G}_{\mathcal{R}}$ are the group velocities of the incident, reflected, and transmitted wave, respectively. Notice that the reflection ratio is equal to 1 when $\omega\gamma\Delta/c > 1$, i.e., for wavenumbers that are only resolvable in the fine region of the grid, a total reflection occurs at the interface point. This agrees with the reflected wave R_2 that is created as P_2 propagates through the resolution change in Figure 2e. As illustrated in Figure 2a, temporal frequency is preserved across the interface point in both of these examples, but wavenumbers are not.

The results from a grid with an abrupt change in resolution can be extended to grids with a gradually changing resolution. In this case, a local wavenumber k_j and a local group velocity \mathcal{G}_j are defined for a given frequency ω and local grid spacing Δ_j using the definitions (7) and (8). Moreover, it is assumed (9) holds at each point in the domain. There are three main results from Vichnevetsky [24] and Long and Thuburn [23] that will be relevant for our purposes. First, no reflections occur if the local group velocity is uniform and not equal to zero as expected. Second, a total reflection occurs for all waves that reach a state of unresolvability on the grid, and the reflection occurs at the point where the local group velocity vanishes ($\mathcal{G}_j = 0$). Thirdly, no reflections occur for globally resolvable wavenumbers in the limit of a smoothly varying grid. The second result implies wave packets analogous to P_2 will still undergo a complete reflection in a gradually changing grid. The third result implies wave packets analogous to P_1 will get *entirely* transmitted through an infinitely smooth resolution change. The commutation error is responsible for the erroneous behavior of P_2 -type waves. The erroneous behavior of P_1 -type waves is an additional issue related to resolution inhomogeneity. Formally speaking, the ‘‘smoothness’’ of the resolution change would reduce error in P_1 -type waves, while a commutation model would reduce errors in P_2 -type waves. The model presented in Section 3.1 addresses both of these issues.

The behavior described here is representative of all energy-conserving numerical schemes with two wavenumbers per frequency. These are among the most common numerical schemes used in turbulence applications (e.g., centered difference, B-splines, finite volume), however, other numerics with difference propagation properties should be discussed. For instance, consider the box scheme whose semi-discretization of (4) is given by,

$$\frac{\partial}{\partial t} \left(\frac{u_j + u_{j+1}}{2} \right) + a \frac{u_{j+1} - u_j}{x_{j+1} - x_j} = 0, \quad (10)$$

and is energy preserving. Instead of reflecting unresolvable scales of motion at higher wavenumbers into the fine region, the box scheme transmits unresolvable scales at lower wavenumbers through the coarse region (similar to an aliasing effect) [25, 26]. The result is still spurious numerical oscillations that need to be suppressed by the commutation model. On the contrary, upwinding schemes do not allow for any reflections in regions of grid inhomogeneity by design. This makes them an attractive candidate for a commutation model that is targeted at mitigating the commutation error. The difficulty with upwinding schemes is that they introduce additional dissipation which must be accounted for by the subgrid stress in order to satisfy

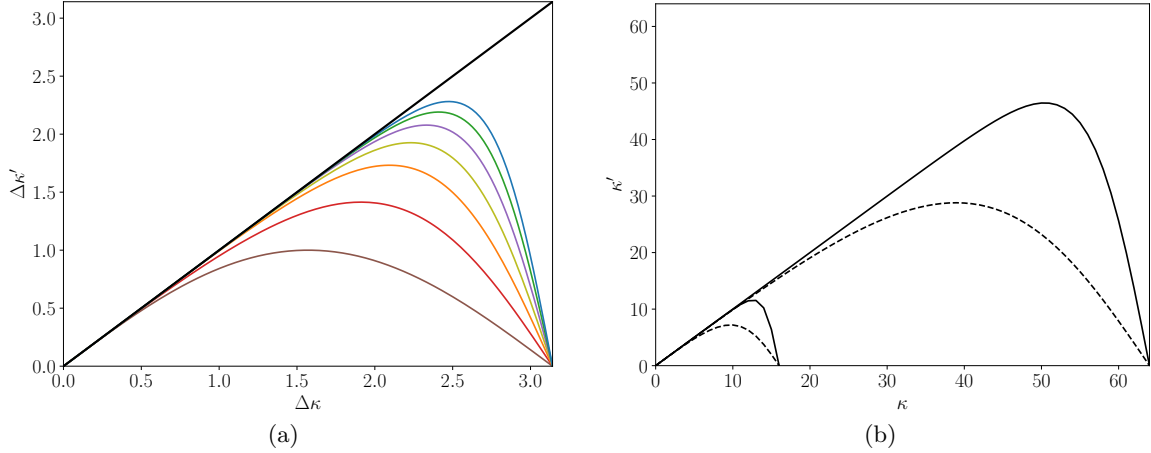


Figure 3: (a) The spectrum of the first derivative operators for a B-spline collocation method of several orders, a second-order centered difference method, and a spectral method; (B_1^2) , (B_1^3) , (B_1^4) , (B_1^5) , (B_1^6) , (B_1^7) , (B_1^{CD}) , (Spectral). (b) The unnormalized spectrum of the B_1^2 and B_1^7 operators for the fine region of the domain with spacing $\Delta_f = \frac{2\pi}{128}$, and the coarse region of the domain with spacing $\Delta_c = \frac{2\pi}{32}$; (B_1^7) , (B_1^2) ,

conservation of energy. An interesting approach may be to use *implicit LES* models in this context, where the leading order error term provides the usual dissipation rate [27, 28], and the upwinding discretization would inherently correct for the commutation error by not allowing for spurious reflections. Lastly, it would be interesting to compare these results with stabilization methods such as the streamline upwind/Petrov-Galerkin method, which was also developed in the context of convection dominated flows [29]. In conclusion, this discussion highlights the connection between the numerics and the behavior of the commutation error. Different implicit filters/discrete derivative operators may require different modeling of the commutation error depending on their numerical propagation properties.

2.2 Impacts of Resolution Inhomogeneity on LES

The effects of resolution inhomogeneity are now demonstrated on the convection of a packet of homogeneous isotropic turbulence through an inhomogeneous grid.

2.2.1 Setup

For this experiment, the resolution change and direction of convection are aligned along a single axis. Without loss of generality, assume this is the x -axis. The linear convection of a three-dimensional field in this setting is governed by,

$$\frac{\partial \bar{\mathbf{u}}}{\partial t} + a_x \frac{\delta \bar{\mathbf{u}}}{\delta x} = 0. \quad (11)$$

Moreover, periodic boundary conditions are used in all three spatial directions.

The implicit filter is defined through a periodic B-spline collocation method in the x -direction and a spectral method in the y - and z -direction. B-splines easily enable the use of inhomogeneous resolution and the study of higher- and lower-order numerical methods, and have been advocated for use in turbulence simulations [30, 15, 31, 32, 33, 34]. Let B_n^k denote the n th derivative B-spline operator of order k , and B_n^{CD} denote the n th derivative second-order centered difference operator. Figure 3a shows the spectrum of the B_1^k operators for $k = 2, 3, \dots, 7$, as well as B_1^{CD} . Figure 3b shows the unnormalized spectrum for the B_1^2 and B_1^7 operators for the fine and coarse regions of the grid considered here. Notice from Figure 3 that B-splines are another example of a numerical scheme that has two possible wavenumbers per frequency. Therefore, we can expect qualitatively similar behavior to the centered difference case analyzed in Section 2.1. A spectral method is used in directions orthogonal to the direction of inhomogeneity to ensure the only erroneous numerical behavior is due to the propagation/reflection of energy from the B-splines. A third-order low storage Runge-Kutta method is used for time advancement [35]. The spurious

reflection/transmission phenomena described in Section 2.1 are independent of temporal discretization, i.e., they depend on spatial discretization alone [36].

A two dimensional slice of the numerical grid is shown in Figure 4a. The propagation direction is of size $[0, 12\pi]$ and is divided into a uniform fine region of size 2π , a uniform coarse region of size 2π , and two regions of gradual grid change that are each of size 4π . The fine resolution spacing is taken to be $\Delta_f = 2\pi/128$, and the coarse spacing is taken to be $\Delta_c = 2\pi/32$. The gradual resolution change is defined through the function,

$$\Delta(x) = \left(1 - \frac{1}{1 + e^{-x}}\right) \Delta_f + \left(\frac{1}{1 + e^{-x}}\right) \Delta_c. \quad (12)$$

Specifically, 105 uniform grid points on the domain $[6\pi/2 - 0.059882471808, 6\pi/2]$ are mapped to the domain $[0, 4\pi]$ through equation (12). The offset value is determined to ensure the points exactly span a 4π interval. The most significant resolution change takes place over much fewer than 105 points and spans a small portion of the 4π interval; however, the length and number of grid points in the gradually changing region are chosen so that the resolution sufficiently approaches the fine and coarse resolutions to satisfy the perfectly matched layer condition [37]. This is necessary for computation of the energy spectra, but would not be an issue in a practical application. Therefore, most of the grid spacing in the gradually changing region is near Δ_f or Δ_c . The coarse region of the domain for the second order B-spline simulation is of size 6π to account for numerical dispersion during the computation of the energy spectra. The two spectral directions are of size $[0, 2\pi]$ and have an effective uniform grid spacing of Δ_f . This setting leads to convection through an *anisotropic*, inhomogeneous grid. This choice is made because the three dimensional commutation error expressed by [1] simplifies to the one dimensional case in this context. Future work will discuss the three-dimensional commutation error and the effect of different grid types in more detail. The current setting is ideal for demonstrating the behavior of the implicit commutation error through the numerical analysis presented in 2.1.

The initial condition is taken to be a ‘packet’ of well-resolved, homogeneous, isotropic turbulence. This packet is analogous to the wave packets studied in the one-dimensional examples in Section 2.1. To create this packet, a fully spectral simulation of a $2\pi \times 2\pi \times 2\pi$ box of homogeneous, isotropic turbulence with 64 uniform grid points in all directions was performed first. A representative instantaneous field from the stationary fully spectral simulation was then placed in the fine region of the domain in the B-spline/spectral simulation and modulated with a Gaussian so that the solution goes smoothly to zero. The choice of 64 grid points in the fully spectral simulation ensures the modulated packet is sufficiently well-resolved by the B-splines in the fine resolution region. In other words, an isotropic spacing of $2\pi/64$ in the fully spectral simulation corresponds to $\Delta_f \kappa_{max} \approx 1.5$ in the B-spline simulation, where $\kappa_{max} = 32$ is the largest nonzero wavenumber in the turbulence packet. As seen by examining the slopes in Figure 3a at the point $(\Delta\kappa) = 1.5$, the entire turbulence packet has positive group velocity initially. As before, this choice is made to help distinguish between absence of \mathcal{C}^I and \mathcal{C}^H .

2.2.2 Results

Seventh-order B-splines and second-order B-splines are examined to illustrate the behavior of higher- and lower-order methods. Results in physical space for seventh-order B-splines are shown in Figure 4. The corresponding energy spectra in the fine and coarse regions of the domain at several stages of the simulation are shown in Figure 5. One-dimensional energy spectra in the x -direction are reported as it best captures the effects of resolution inhomogeneity in that direction. The initial packet of turbulence is shown in Figure 4b, and the dashed line gives the corresponding energy spectrum in Figure 5. We refer to wavenumbers $|\kappa| \in [0, 16]$ as the *coarse wavenumbers*, wavenumbers $|\kappa| \in (16, 32]$ as the *fine wavenumbers* and wavenumber $|\kappa| \in (32, 64]$ as the *spurious wavenumbers*. The fine region of the domain is capable of representing the fine, coarse, and spurious wavenumbers, while the coarse region is only capable of representing the coarse wavenumbers. The initial packet of turbulence only contains fine and coarse wavenumbers, so any energy transferred to higher wavenumbers by the resolution inhomogeneity is indeed spurious.

All the resolved scales of motion have positive group velocity initially, so the entire turbulence packet travels to the right through the fine region at a velocity near the convection velocity for both B-spline orders. Upon interaction with the resolution change, newly unresolvable scales of motion are reflected back into the fine resolution region at higher wavenumbers in the spurious wavenumber regime with negative group velocity. Figure 4c shows a scaled version of these high wavenumber reflections in physical space. The corresponding

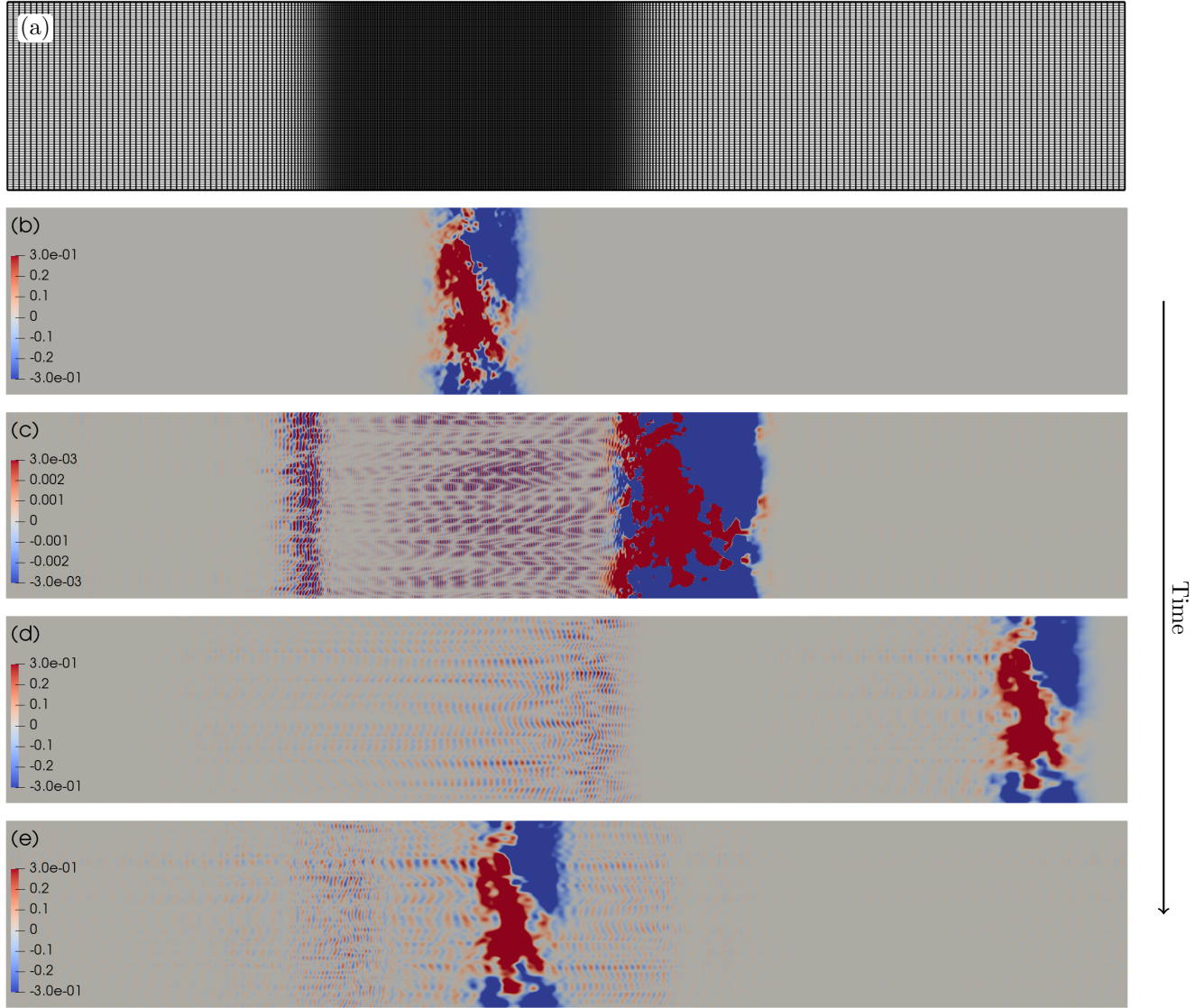


Figure 4: Convection of a packet of homogeneous, isotropic turbulence through an anisotropic, inhomogeneous grid with seventh-order B-splines and a convection velocity of 1. (a) A slice of the numerical grid. (b), (c), (d), and (e) show the streamwise velocity field at times 0.00, 7.81, 18.75, and 39.06, respectively.

spectra in Figure 5a show how the energy from the fine wavenumbers is concentrated in a narrow band of spurious wavenumbers according to the effective wavenumber for each B-spline order. Moreover, the speed of the reflections is much greater for seventh-order B-splines than second-order B-splines. Interestingly, we found that the ratio of the group velocity to convection velocity of the highest wavenumber reflections for each B-spline order matches the order of the B-spline (e.g., the Nyquist wavenumber propagates at negative N times the convection velocity for N th order B-splines). This result is a special property of B-splines that deserves a rigorous proof. Similarly, [38] demonstrated that an infinite speed of reflection occurs for spectral numerics. In this sense, the issues associated with resolution inhomogeneity do not get better with higher-order numerics as one may expect but get worse. The realization that the issues associated with inhomogeneity do not go away with higher-order numerical schemes, and may even be considered to get worse, arises from the fact that the commutation error is not a numerical artifact, but a fundamental error with the governing LES equations that manifests through the propagation properties of the underlying

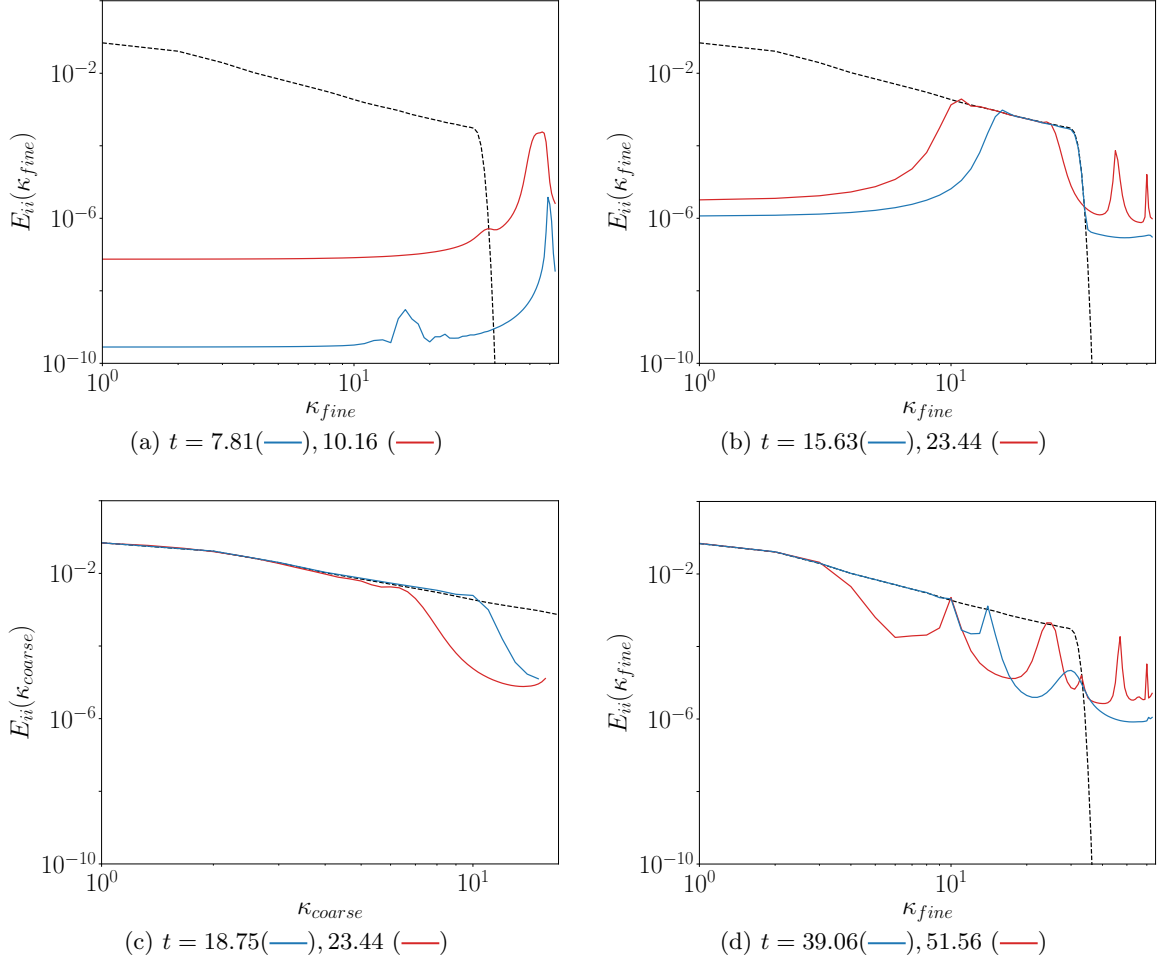


Figure 5: One dimensional energy spectra, E_{ii} , in the direction of inhomogeneity at different times t ; κ_{fine} and κ_{coarse} represent the wavenumbers in the fine and coarse regions of the domain, respectively. (a) High wavenumber reflections propagating backward through the fine region corresponding to the energy in the fine region in Figure 4c. (b) The subsequent reflections propagating forward through the fine region corresponding to the energy in the fine region in Figure 4d. (c) The spectra of the resolved turbulence packet in the coarse region corresponding to the energy in the coarse region in Figure 4d. (d) The spectra of the turbulence packet after one flow through corresponding to the energy in the fine region in Figure 4e. — (7th order B-splines), — (2nd order B-splines), - - - (Initial spectra of the turbulence packet shown in Figure 4b).

numerical methods. Accordingly, problems related to resolution inhomogeneity are inherently a modeling issue. This discussion also highlights the distinction between discretization error and the commutation error.

Once the reflected spurious scales of motion reach the resolution change on the left side of the fine region, they are subsequently reflected into the fine region with positive group velocity at their initial fine wavenumber counterpart. These secondary reflections occur in the fine wavenumber regime but are as erroneous as the spurious reflections that created them. This stage is shown in Figure 4d and 5b. For both B-spline orders, the energy spectra in the fine resolution region for the initial turbulence packet and the reflected scales of motion match for all fine wavenumbers. This indicates a total reflection of all scales that are only representable on the fine grid. This observation agrees with our discussion of the P_1 wave discussed in Section 2.1. Without the properly tuned commutation terms, this cycle of reflection between fine and spurious wavenumbers repeats. The energy initially contained in the fine wavenumbers gets trapped in the fine resolution region.

The only scales of motion that make it through to the coarse region are those that can be represented

on the coarse grid, i.e., the coarse wavenumbers. These scales are shown in Figure 4d on the right-hand side of the domain and Figure 5c. The energy spectra at the initial time, and after the packet has convected into the coarse region, match *almost* identically for all coarse wavenumbers. The discrepancy in the highest coarse wavenumbers coincides with the negative group velocity region shown in Figure 3a and is expected/unavoidable. Moreover, a relatively small amount of the low, coarse wavenumber scales also get trapped in the fine region, as shown in Figure 5b. These scales correspond with the P_1 wave discussed in Section 2.1, and would vanish in the limit of a smoothly varying grid. The amount of transmitted/reflected energy in these scales corresponds with the reflection ratio.

The trapped scales of motion in the fine region of the domain are physically incorrect and numerically problematic. An increase in high wavenumber energy can lead to numerical stability issues, and the trapped low wavenumber energy can corrupt otherwise meaningful statistics. Moreover, nonlinear effects in the full Navier-Stokes equations would magnify these issues as erroneous scales of motion would interact with and contaminate any other incoming turbulence. This is seen by considering the turbulence packet after one flow through, as shown in Figure 4e. As the coarsely resolved packet re-enters the fine region (without any active forcing turned on), the spectrum in the fine region gets corrupted by the trapped fine wavenumber energy, as shown in Figure 5d.

3 Commutation Modeling

3.1 Model Formulation

Ghosal and Moin [1] developed a procedure for generating terms of the commutation error that can be added to the governing equations to correct for the commutation error up to any order in filter width. First, they defined filtering on a nonuniform grid through a mapping function f that maps physical space (with nonuniform grid spacing $\Delta(x)$) into a computational space (with uniform grid spacing δ). The commutation error was then expressed in terms of this mapping function through an integral expression. Lastly, the commutation integral was inverted via a Taylor series expansion to generate terms of the commutation error up to a given order in filter width. Similarly, the filtered field was related to the unfiltered field through a Taylor series expansion. Their analysis led to the following series for the N th order one dimensional commutation error:

$$\mathcal{C}^I(u) = -M_2\Delta \frac{d\Delta}{dx} \frac{\partial^2 \bar{u}}{\partial x^2} + \left(\frac{M_2^2}{2} - \frac{M_4}{6} \right) \Delta^3 \frac{d\Delta}{dx} \frac{\partial^4 \bar{u}}{\partial x^4} + \dots + C_M \Delta^{N-1} \frac{d\Delta}{dx} \frac{\partial^N \bar{u}}{\partial x^N} + \mathcal{O}(\kappa\delta)^{N+2}. \quad (13)$$

where M_k is the k th order moment of the filter, N is even, and (for simplicity) C_M is a constant that depends on the moments of the filter.

The analysis of Ghosal and Moin [1] is essentially an approximate deconvolution technique for modeling the commutation error based on a Taylor series expansion [39], and does not apply to filters that actually discard information, e.g., implicit filters [40]. For instance, it requires that all moments of the filter converge. Moments of the implicit filter cannot be adjusted to correct for the commutation error as in Vasilyev et al. [3], so we must rely on explicit commutation modeling through the SGS tensor. Moreover, the analysis of Ghosal and Moin [1] relied on a dimensionally inconsistent assumption that led to the absence of several terms of the commutation error. Specifically, it is assumed that $\delta \ll \kappa\delta$, for all wavenumbers κ . This assumption is dimensionally inconsistent as $\delta \sim L$ and $\kappa \sim 1/L$ for some length scale L . Although this series does not directly apply to implicit filters, it is important to correct for this inconsistency for furthering our understanding of the commutation error. In appendix A, a complete commutation series is derived. We also show the general structure of the N th order commutation error is given by:

$$\mathcal{C}^I(\psi) = \sum_{n=1}^{N/2} \sum_{m=1}^{2n} C_{nm} \Delta^{2n-m} \left[\frac{\partial^{2n-m+1} \bar{\psi}}{\partial x^{2n-m+1}} \right] \frac{d^m \Delta^m}{dx^m} + \mathcal{O}(\delta^{N+2}), \quad (14)$$

for even N and constants C_{nm} . Additional dispersive and dissipation terms arise when considering (14) instead of (13).

A commutation model must filter scales approaching a state of unresolvability in regions of the grid with inhomogeneous resolution. Although (14) does not formally apply to implicit filters, we can use it to suggest a general form for a commutation model, which is then adjusted based on the insights and numerical

properties of the commutation error discovered in section 2. In [1], it is assumed that $\kappa\delta < 1$ so that the higher order terms of (13) can be ignored. For implicit filters, $0 \leq \kappa\delta \leq \pi$ so this is not true for all scales. In fact, notice that the most significant commutation term for large $(\kappa\Delta)$ will yield the most useful term for filtering out high wavenumber content that cannot be resolved in coarser regions of the grid. This is particularly advantageous for the types of numerical schemes considered as here where unresolvable scales get reflected at even higher wavenumbers. Substituting $\psi = \hat{\psi}e^{i\kappa x}$ into (14) shows the most significant commutation term of (14) (and incidentally (13)) for $(\kappa\Delta)$ large is:

$$a\mathcal{E}^I(\psi) \approx Ca \frac{i^N}{\Delta} \frac{d\Delta}{dx} (\kappa\Delta)^N \bar{\psi} = (-1)^{N/2} Ca \Delta \frac{d\Delta}{dx} \left(\Delta^{N-2} \frac{\partial^N \bar{\psi}}{\partial x^N} \right), \quad (15)$$

for some constant C and even order N (N is assumed to be a positive even integer for the remainder of this paper). For different discretizations, (14) may suggest other useful model terms to include. For now, equation (15) is used as the basis for developing a commutation model and deserves consideration.

First, notice that a typical SGS model such as the Smagorinsky model would not sufficiently correct for the commutation error, because the characteristic time scale is no longer the turbulent time scale, but rather the time scale defined through the convection velocity, the rate of change of grid resolution, and the grid resolution itself (this can also be seen by examining equation (16) below). The commutation model given by (15) includes both of these dependencies through the viscosity $\nu_{comm} = a\Delta(d\Delta/dx)$. On the other hand, the $(\Delta^{N-2}\partial^N\bar{\psi}/\partial x^N)$ part of the model acts as a filter for the scales that must be removed. For $N = 2$, (15) represents an additional viscous term. For $N > 2$, (15) is a hyperviscosity model, which is expected for approximate deconvolution methods based on a Taylor series expansion.

Second, notice that the larger N , the more significant (15) is for large wavenumbers. If we could take $N \rightarrow \infty$, equation (15) would essentially act as a sharp spectral filter that could be designed to remove scales approaching unresolvability without affecting scales that will maintain resolvability. However, the number of available derivatives of the filtered field limits how sharp (15) can be, i.e., the underlying numerics constrain N based on the number of accessible derivative operators. For example, CFD codes typically only have access to second derivative operators so that N would be limited to 2. Therefore, for any finite value of N , there is always a trade-off between removing high wavenumber scales in fine regions of the grid that are approaching unresolvability, and preserving the well-resolved wavenumber scales in coarse regions of the grid. Larger values of N perform better within the context of this trade-off than smaller values of N . Accordingly, our one-dimensional model for resolution inhomogeneity takes the form of (15) with the largest possible value of N . Furthermore, larger values of N require not only higher order numerics but also additional boundary conditions and potentially different stability conditions, which are often mentioned as a problem with hyperviscosity models. The methods proposed in 3.1.1 and 3.1.3 give a way of overcoming these difficulties, which is useful for the commutation model present here as well as general hyperviscosity models. Lastly, the model coefficient attached to (15) will need to be calibrated based on the numerical behavior of the commutation error. This is addressed in Section 3.1.2.

Before discussing further model developments, it is important to note that, as with all approximate deconvolution techniques, the commutation model proposed by Ghosal and Moin [1] is aimed at reconstructing the instantaneous commutation error. While this is appropriate for certain problems such as the linear advection problem considered here, a commutation model for practical LES applications may require a statistical formulation (e.g., it is well known that similarity models are highly correlated with subgrid scales, but do not perform well as a SGS model without inclusion of an eddy viscosity to capture the dissipation rate [41, 7].) A statistical description of the commutation error arises from considering a box of homogeneous isotropic turbulence with cut off wavenumber $\kappa_c(t)$ that varies with time. The change in resolved turbulent kinetic energy is:

$$\frac{\partial}{\partial t} \int_0^{\kappa_c(t)} E(\kappa, t) dk = E(\kappa_c(t), t) \frac{\partial \kappa_c}{\partial t}(t) + \int_0^{\kappa_c(t)} \frac{\partial E(\kappa, t)}{\partial t} dk. \quad (16)$$

The commutation error is statistically equivalent to ignoring the first term on the right-hand side of (16). This term is the total production/destruction of resolved turbulent kinetic energy due to the commutativity between filtering and differentiation. In an LES, a commutation model must capture this dissipation rate. For instance, for a Kolmogorov spectrum, $E(\kappa_c(t), t) \frac{\partial \kappa_c}{\partial t} = C_k \varepsilon^{2/3} \kappa_c(t)^{-5/3} \frac{\partial \kappa_c}{\partial t}$. This approach could be used to tune commutation models and constants in LES applications. Furthermore, (16) suggests other forms of

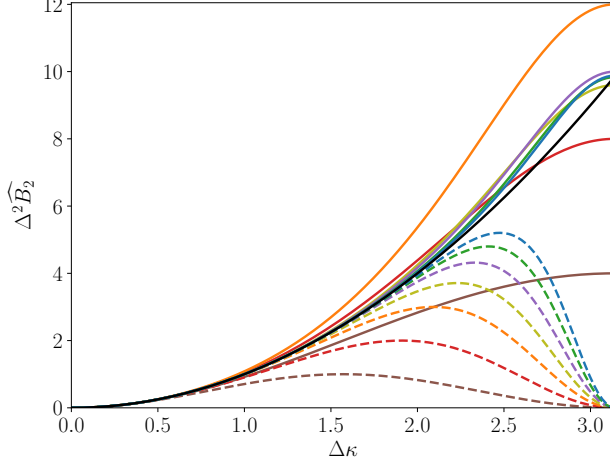


Figure 6: The spectrum of the second derivative operators (\widehat{B}_2) for a B-spline collocation method of several orders, a second-order centered difference method, and a spectral method. Repeated application of the first derivative operators are shown by the corresponding dashed lines; --- , --- ($B_2^2, B_1^2 B_1^2$) --- , --- ($B_2^3, B_1^3 B_1^3$) --- , --- ($B_2^4, B_1^4 B_1^4$) --- , --- ($B_2^5, B_1^5 B_1^5$) --- , --- ($B_2^6, B_1^6 B_1^6$) --- , --- ($B_2^7, B_1^7 B_1^7$) --- , --- ($B_2^{CD}, B_1^{CD} B_1^{CD}$) --- (Spectral).

commutation models aside from those proposed by [1] may be appropriate for addressing the commutation error in LES. For instance, perhaps a structure-function model based on capturing the value of the spectrum at the cut off wavenumber could be combined ν_{comm} to satisfy (16). Future work will investigate structural versus functional modeling for the commutation error in LES as well as other modeling techniques. Note that (16) does not account for the numerical effects associated with convection through inhomogeneous resolution, which will still need to be considered when addressing the commutation error in realistic applications.

3.1.1 $B_2 - B_1 B_1$ Filter

Let $F_N(\psi) \approx \partial^N \psi / \partial x^N$ represent a general numerical operator approximating the N th derivative. The commutation model (15) can then be written as:

$$\mathcal{E}^I(\psi) \approx (-1)^{N/2} C \Delta \frac{d\Delta}{dx} (\Delta^{N-2} F_N(\bar{\psi})) . \quad (17)$$

As mentioned above, it is desirable to take N large, but the underlying numerics often limits N . However, numerical operators can be designed to mimic hyperviscosities without increasing the order of the differential equation. Specifically, lower-order differential operators can be combined to create higher order filters.

Consider the operator given by the difference between the numerical second derivative operator, B_2 , and repeated application of the numerical first derivative operator, $B_1 B_1$, (for a general numerical scheme). Figure 6 shows each of these operators for centered difference numerics and several orders of B-splines. A simple Taylor expansion shows for centered difference numerics:

$$\begin{aligned} (B_2^{CD} - B_1^{CD} B_1^{CD})u &\equiv \frac{u_{j+1} - 2u_j + u_{j-1}}{\Delta^2} - \frac{u_{j+2} - 2u_j + u_{j-2}}{4\Delta^2} = \frac{\Delta^2}{12} \frac{d^4 u}{dx^4} - \frac{\Delta x^2}{3} \frac{d^4 u}{dx^4} + \mathcal{O}(\Delta^4) \\ &\equiv \frac{-u_{j+2} + 4u_{j+1} - 8u_j + 4u_{j-1} + u_{j-2}}{4\Delta^2} = -\frac{\Delta^2}{4} \frac{d^4 u}{dx^4} \mathcal{O}(\Delta^4) \\ &\sim \Delta^2 F_4(\psi) + \mathcal{O}(\Delta^4) \end{aligned} , \quad (18)$$

Similarly, it can be shown that

$$(B_2^7 - B_1^7 B_1^7)\psi \sim \Delta^8 \frac{d^{10}\psi}{dx^{10}} = \Delta^8 F_{10}(\psi) \quad (19)$$

$$(B_2^2 - B_1^2 B_1^2)\psi \sim \Delta^2 \frac{d^4\psi}{dx^4} = \Delta^2 F_2(\psi) \quad (20)$$

Notice how in all of these cases, $B_2 - B_1 B_1 \sim \Delta^{N-2} F_N$ for some value of N , which corresponds exactly to the form of the model correction given by (17); i.e.,

$$\mathcal{E}^I(\psi) \approx (-1)^{N/2} C \Delta \frac{d\Delta}{dx} (B_2 - B_1 B_1) \bar{\psi}. \quad (21)$$

The $B_2 - B_1 B_1$ filter allows for the inclusion of higher order commutation terms without changing the order of the differential equation. This avoids the use of higher order numerical methods and the need for additional boundary conditions. We note that Iovieno and Tordella [5] also developed an approach for including up to the fourth order commutation terms in the governing equations without changing the order of the equations. Their approach relied on multiple levels of filtering using a specific volume average formulation of the equations, which depended on the analysis of Ghosal and Moin [1] holding for the filter. While their approach does not hold for the implicit filter and is limited to the fourth order terms, they also mentioned the benefits of explicit commutation modeling and the inclusion of higher order terms without raising the order of the equations. Furthermore, the $B_2 - B_1 B_1$ filter is particularly useful because the first and second differential operators are already required by the governing equations, and are thus readily available in practical applications.

Moreover, the $B_2 - B_1 B_1$ operator makes intuitive sense. Compare the second derivative operator, B_2 , with repeated application of the first derivative operator, $B_1 B_1$, in Figure 6; for numerically well-resolved wavenumbers, the B_2 and $B_1 B_1$ operators are almost identical, and they cancel out. However, for insufficiently resolved wavenumbers, their difference is nonzero and filters out higher wavenumbers. In essence, the $B_2 - B_1 B_1$ operator acts as an indicator for the scales that are not sufficiently representable by the underlying numerics. The ability to detect and filter insufficiently resolved scales of motion may be of great value for not only addressing issues related to the commutation error but also a wide range of numerical issues in LES modeling. For implicit commutation error, the $B_2 - B_1 B_1$ model allows for sharper filters and can detect scales with negative group velocity. The $B_2 - B_1 B_1$ model can also be used as a correction for discretization error. Ghosal [13], Chow and Moin [14], and Kravchenko and Moin [15] showed that discretization error can significantly overwhelm errors in the SGS term and, therefore, must be corrected. The $B_2 - B_1 B_1$ model is a natural filter for discretization error and adapts to the underlying numerics without needing to define ad hoc filter widths or using explicit filters that introduce additional error such as the violation of Galilean invariance and conservation of energy (i.e., ‘false-dissipation’) [10]. This aligns with previous work suggesting the use of hyperviscosities for the correction of discretization error [18]. Future work will investigate the use of these numerics operators to correct for discretization error. The focus remains on the implicit commutation error for now.

3.1.2 Model Coefficient

A coefficient for the implicit commutation model developed above is derived in Appendix B and is repeated here:

$$C = \frac{(-1)^{\frac{N-2}{2}} \log(\varepsilon)}{\left(\frac{\max(\Delta) - \min(\Delta)}{\max(\Delta)}\right) \left(\Delta^N \hat{F}_N(\kappa_a)\right)}. \quad (22)$$

This coefficient is specific to the linear advection problem outlined in Section 2.2.1 and will need to be adjusted depending on the application. For instance, in LES it would be possible to use (16) to calibrate the model coefficient for a Kolmogorov spectrum to produce the correct transfer rate to the subgrid scales in regions of grid inhomogeneity. However, this approach is not appropriate for the linear convection problem considered here. Therefore, we highlight a few important characteristics of the coefficient derived in appendix B which we believe will be important for all applications.

First, ε is a tolerance level indicating the desired amount of reduction in the energy in reflections. This is a measure of the tradeoff between dissipating erroneous reflections in fine regions of the grid and preserving

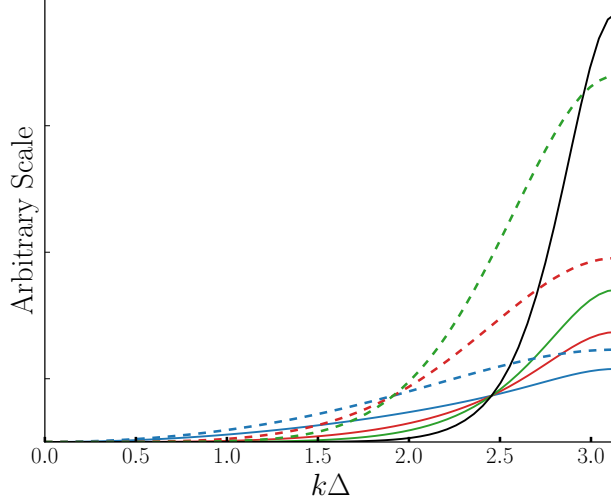


Figure 7: Examples of the commutation model with constant C determined by (22). The scale is arbitrary and depends on ε and $d\Delta/dx$. — (solid blue) ($F_2 = B_2^7$), — (solid red) ($F_4 = B_4^7$), — (solid green) ($F_6 = B_6^7$), — (solid black) ($\Delta^8 F_{10} \sim B_2^7 - B_1^7 B_1^7$), - - - (dashed blue) ($F_2 = B_2^2$), - - - (dashed red) ($\Delta^2 F_4 \sim B_2^2 - B_1^2 B_1^2$), - - - (dashed green) ($F_6 = (B_2^2)^3$).

well-resolved wavenumbers in coarse regions of the grid. For a LES application, (16) indicates that there may be an optimal value of this tradeoff that provides the correct transfer rate to the subgrid scale. For the linear advection case, it is demonstrative to examine how the commutation model behaves for several different values of ε .

Second, $\hat{F}_N(\kappa)$ represents the spectrum of F_N evaluated at the wavenumber κ . \hat{F}_N is used as opposed to $(i\kappa)^N$ to further account for numerical effects. Notably, we use the value of \hat{F}_N at the apex wavenumber κ_a . This choice is made to take advantage of how the commutation error manifests numerically. To elaborate, the constant is designed to kill off wavenumbers quickly *after* they have been reflected at higher wavenumbers. By targeting the reflections, we obtain a larger separation between the scales of motion we need to filter out, and those we need to preserve. This exploit is especially advantageous for low values of N where the filters produced from (15) are not particularly sharp. The lower the wavenumber with positive group velocity, the higher the wavenumber of the reflection with negative group velocity. Accordingly, the smallest wavenumber with nonpositive group velocity is dissipated the least from the model correction term. Therefore, we evaluate \hat{F}_N at κ_a in (22). In essence, it is more advantageous to use a model to correct for the absence of \mathcal{C}^I in this problem, than to directly model \mathcal{C}^I . In LES, more work is needed to see if a similar exploit can be performed. For example, nonlinearity may require scales to be removed before reflection, but this would also lead to more dissipation of the resolvable turbulence with the filters considered here. If the scales are to be removed before reflection, the constant should be based on the cutoff wavenumber in the coarse resolution region instead of κ_a .

Lastly, the ratio of the group velocity to convection velocity was also used in determining the model constant. This further emphasizes the importance of including numerical properties in the formulation of the commutation model and SGS models in general.

The spectrum of the commutation model with this choice of coefficient and the filters described in Section 3.1.1 is shown in Figure 7. The model for second- and seventh-order B-splines with several different choices of N is shown. For an arbitrary tolerance value of ε , the model coefficient creates an intersection point at κ_a between different orders of N . Moreover, this intersection point shifts depending on the order of the underlying numerics. Figure 7 highlights how larger values of N lead to more desirable forms of the model. As N increases, reflected scales are dissipated more, and resolvable scales are better preserved.

As shown in Section 3.2, this constant performs quite well in practice. However, for a more conservative estimate, the wavenumber κ used to calibrate the constant can be reduced slightly, or ε can be increased.

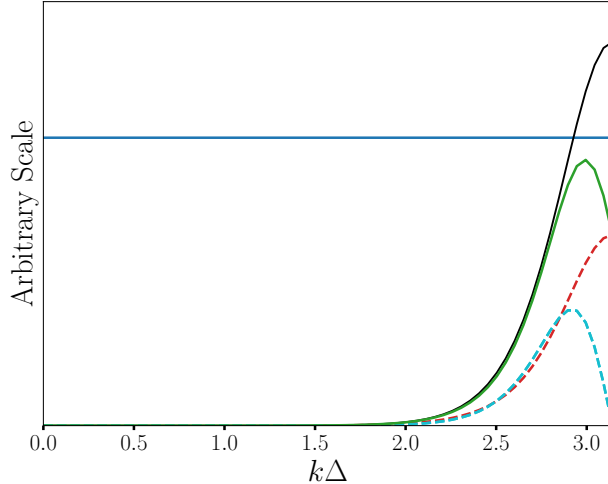


Figure 8: An approximation to a tenth order dissipation term/filter that also satisfies CFL constraints. The fact that the B_1 operator goes to zero at the Nyquist frequency is exploited to reduce dissipation in the highest wavenumbers where differentiation is not meaningful for non-spectral numerics anyways. — $(\Delta^8 F_{10} \sim (B_2^7 - B_1^7 B_1^7))$, — (CFL Operator Threshold), - - - $(6 \times 10^{-10} \Delta^9 (B_1^7)^4 (B_2^7)^5)$ - - - $((3.0 \times 10^{-4}) \Delta^9 (B_2^7)^8)$, — $(F_{10} = (3 \times 10^{-4} (B_2^7)^5 + 6 \times 10^{-10} (B_1^7)^4 (B_2^7)^6)$

3.1.3 CFL Constraints

We mentioned that the number of accessible derivative operators limits N , however, stability constraints also limit N . Larger values of N amount to adding higher order dissipation. If the model is treated explicitly, this could potentially interfere with CFL constraints. In this case, either N should be taken as large as possible without interfering with stability, or the form of numerical operators can be further exploited to design numerically stable higher order dissipation operators. The former approach is analyzed further.

The fact that the B_1 operator goes to zero at the Nyquist wavenumber can be used to create high order numerical filters that do not affect CFL conditions. Consider the explicit Euler discretization of the equation $\partial_t \hat{u} = f(\kappa) \hat{u}$, i.e., $\hat{u}^{n+1} = (1 + \Delta t f(\kappa))^n \hat{u}_0$, for general operator $f(\kappa)$. The restriction on the amplification factor places an upper bound on the norm of the operator $f(k)$, i.e., $\|f\|_\infty \leq 2/\Delta t$. Higher order corrections to the commutation error may violate these types of CFL restriction, although such a large dissipation in the highest wavenumbers is not necessary. Figure 8 demonstrates an example of this behavior with the $N = 10$ correction given by the $\Delta^8 F_{10} \sim (B_2^7 - B_1^7 B_1^7)$ operator shown previously in Figure 7. This operator violates the given CFL constraint by adding too much dissipation in the highest wavenumbers. Instead, consider the operator, $F_{10} \approx 3 \times 10^{-4} (B_2^7)^5 + 6 \times 10^{-10} (B_1^7)^4 (B_2^7)^6$, also shown in Figure 8. This operator behaves like the tenth order correction to the commutation error for most wavenumbers, and will kill off all reflected wavenumbers by at least ε , as desired. Moreover, it is numerically stable with the given CFL constraint because the dissipation is reduced slightly in the highest wavenumbers. Notice how the behavior of the B_1 operator ensures the CFL operator threshold is not breached.

In general, the highest wavenumbers are poorly represented by any non-spectral numerical method and large dissipation in these wavenumbers is responsible for numerical instability. Since numerical differentiation is not meaningful in these wavenumbers, lowering the dissipation to satisfy a CFL constraint is valid. However, one cannot rely solely on the B_1 operator because then the dissipation at the Nyquist frequency will drop to zero, which will lead to other numerical instabilities. Therefore, the approach discussed here is a useful way to explicitly treat viscosity and hyperviscosity models, without affecting the CFL condition.

3.2 Model Results

Define the local grid spacing as $\Delta(x) = (\Delta_x(x), \Delta_y, \Delta_z)$. The model (17) is introduced into equation (11) as

$$\frac{\partial \bar{\mathbf{u}}}{\partial t} + a_x \frac{\delta \bar{\mathbf{u}}}{\delta x} = -(-1)^{\frac{N}{2}} C \Delta_x \left(a_x \frac{\partial \Delta_x}{\partial x} \right) (\Delta_x^{N-2} F_N(\bar{\mathbf{u}})), \quad (23)$$

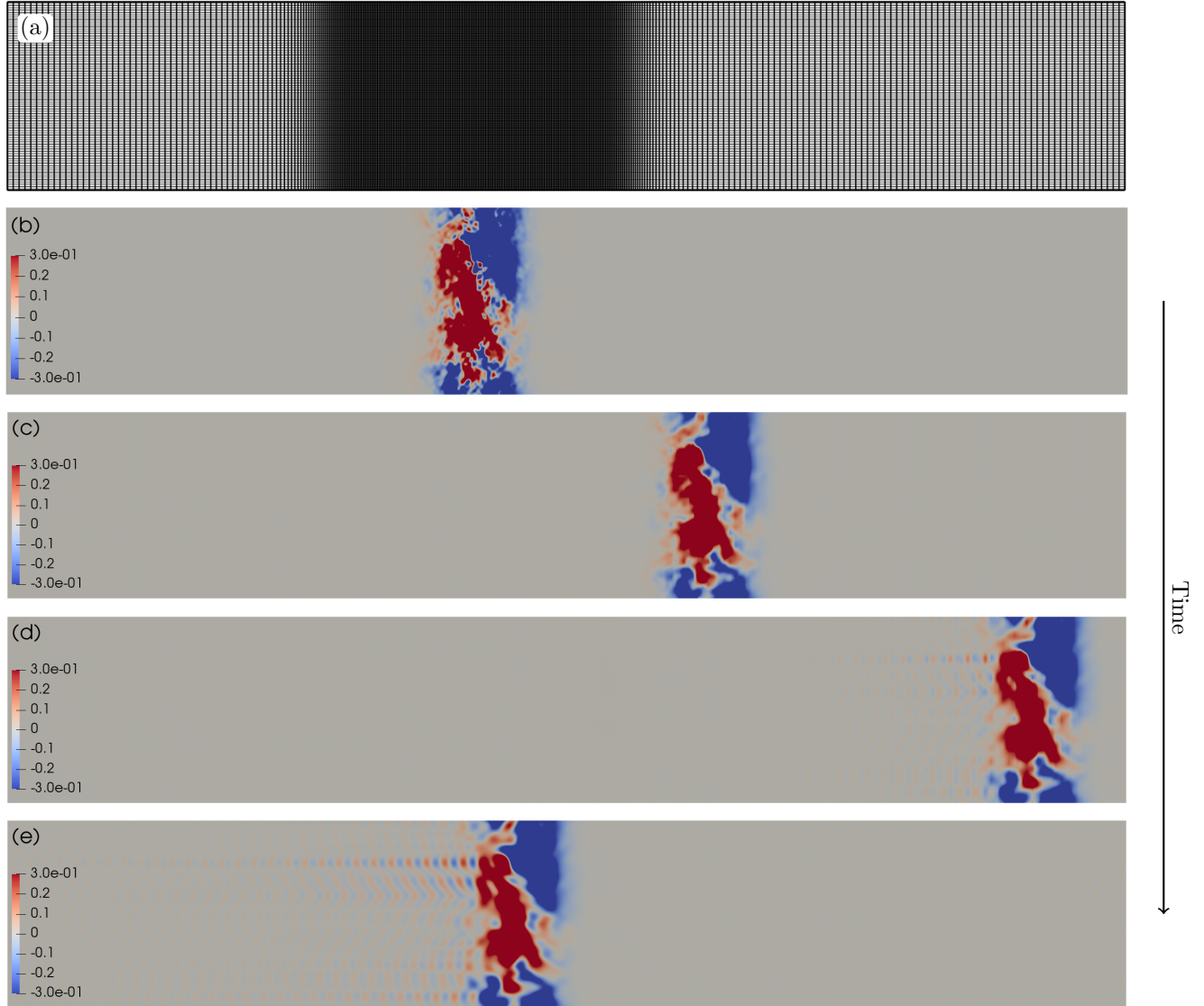


Figure 9: Convection of a packet of homogeneous, isotropic turbulence through an anisotropic, inhomogeneous grid with seventh-order B-splines, a convection velocity of 1, and a commutation model with $F_{10} = \Delta^8(B_2^7 - B_1^7 B_1^7)$ and $\varepsilon = 0.001$. (a) A slice of the numerical grid. (b), (c), (d), and (e) show the streamwise velocity field at times 0.00, 7.81, 18.75, and 39.06, respectively.

where the constant C is given by (22), and the operator F_N approximates the N th derivative in the x -direction, i.e., $F_N \approx (\partial^N / \partial x^N)$. Recall, the dependence on x in (23) comes from the fact that the three-dimensional commutation error simplifies to the one-dimensional case when the resolution inhomogeneity is only in the x -direction. The ability of the model to correct for the issues related to resolution inhomogeneity is tested in the same setting described in Section 2.2.

For the seventh-order B-spline results, three different choices of N and ε are tested: $N = 2$ corresponding to the second derivative operator $F_2 = B_2^7$ with $\varepsilon = 0.1$, $N = 4$ corresponding to the fourth derivative operator $F_4 = B_4^7$ with $\varepsilon = 0.01$, and $N = 10$ corresponding to the $\Delta^8 F_{10} \sim B_2^7 - B_1^7 B_1^7$ operator with $\varepsilon = 0.001$. For the second-order B-spline results, two choices of N are tested for both $\varepsilon = 0.1$ and $\varepsilon = 0.001$: $N = 2$ corresponding to the $F_2 = B_2^2$ operator, and $N = 4$ corresponding to the $\Delta^2 F_4 \sim B_2^2 - B_1^2 B_1^2$ operator. These values, along with the model coefficients, are listed in Table 1.

N	F_N	ε	C
2	B_2^7	0.1	0.489863408538
4	B_4^7	0.01	0.147454712123
10	$\Delta^8(B_2^7 - B_1^7 B_1^7)$	0.001	8.62777909298
2	B_2^2	0.1	0.764465587675
2	B_2^2	0.001	2.29339676302
4	$\Delta^2(B_2^2 - B_1^2 B_1^2)$	0.1	1.5228300657
4	$\Delta^2(B_2^2 - B_1^2 B_1^2)$	0.001	4.56849019709

Table 1: Model Constants.

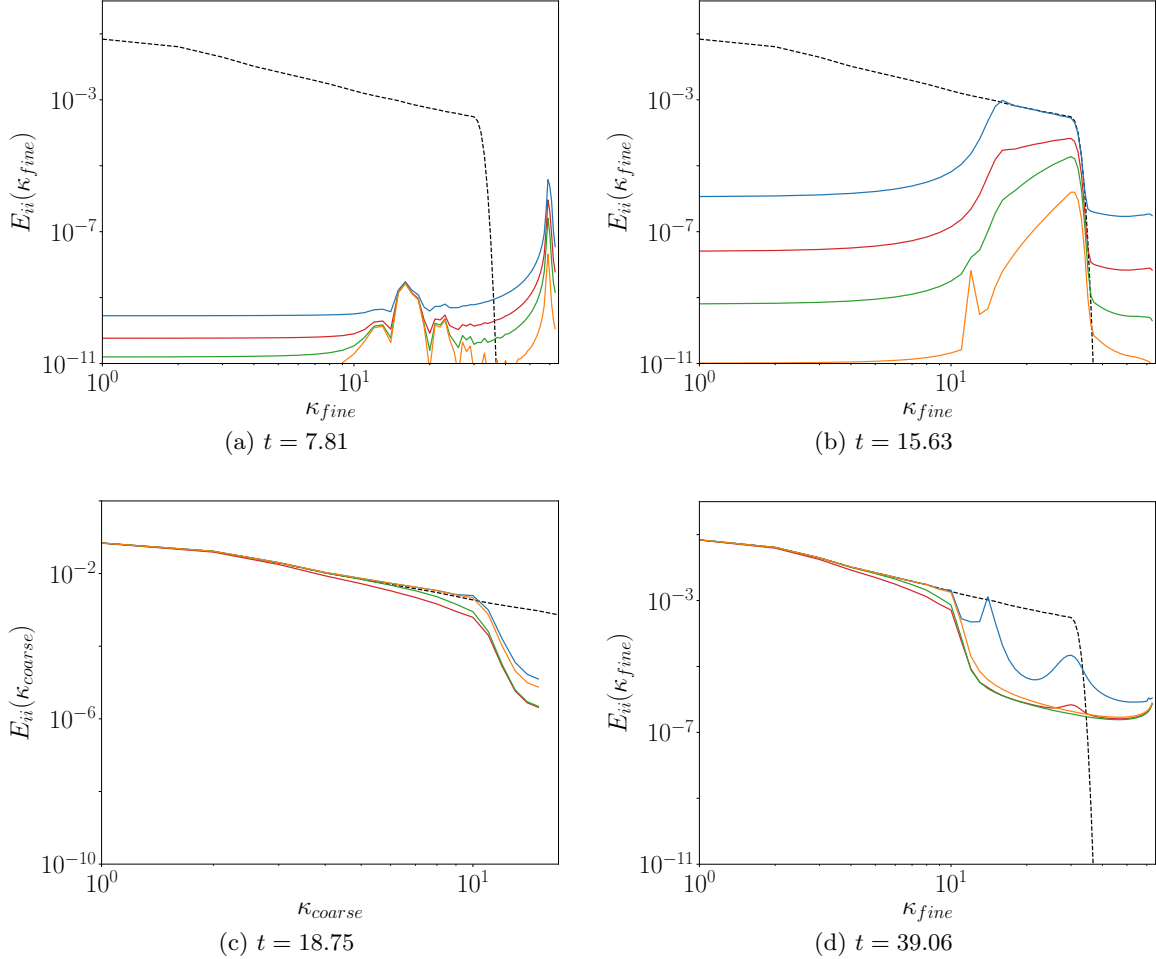


Figure 10: Energy spectra, E_{ii} , in the direction of convection at different times t for 7th order B-splines; κ_{fine} and κ_{coarse} represent the wavenumbers in the fine and coarse regions of the domain, respectively. (a) High wavenumber reflections propagating backward through the fine region. (b) The subsequent reflections propagating forward through the fine region. (c) The spectra of the resolved turbulence packet in the coarse region. (d) The spectra of the turbulence packet after one flow through. — (No model), — ($F_2 = B_2^7$, $\varepsilon = 0.1$), — ($F_4 = B_4^7$, $\varepsilon = 0.01$), — ($F_{10} \sim \Delta^8(B_2^7 - B_1^7 B_1^7)$, $\varepsilon = 0.001$), - - - (Initial Packet)

For seventh-order B-splines, ε is taken to decrease with N , whereas for the second-order B-splines, each value of N is tested at the same two values of ε . In this sense, the seventh-order B-spline results demonstrate how the model can afford more dissipation in the high wavenumbers as N increases without sacrificing

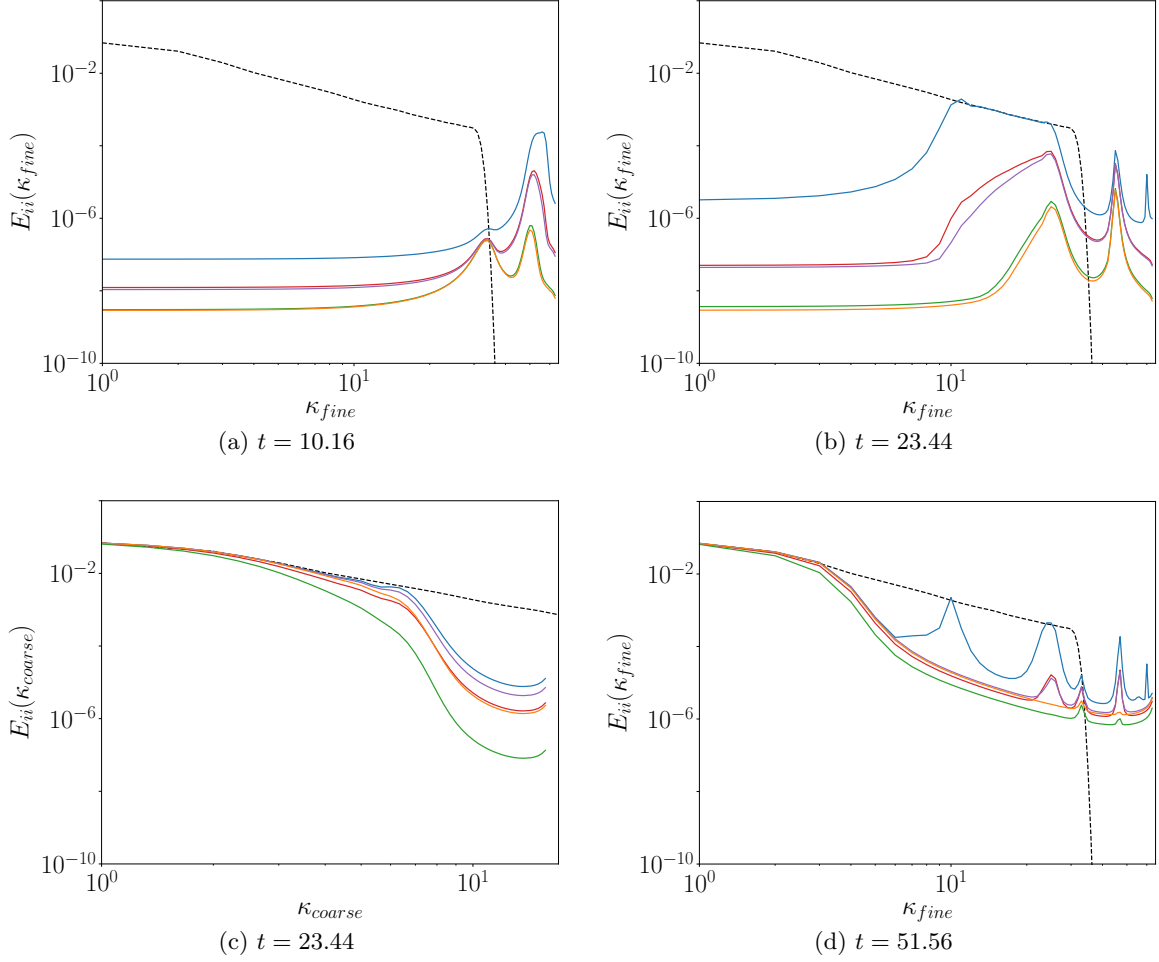


Figure 11: Energy spectra, E_{ii} , in the direction of convection at different times t for 2nd order B-splines; κ_{fine} and κ_{coarse} represent the wavenumbers in the fine and coarse regions of the domain, respectively. (a) High wavenumber reflections propagating backward through the fine region. (b) The subsequent reflections propagating forward through the fine region. (c) The spectra of the resolved turbulence packet in the coarse region. (d) The spectra of the turbulence packet after one flow through. — (No model), — ($F_4 \sim \Delta^2(B_2^2 - B_1^2 B_1^2)$, $\varepsilon = 0.1$), — ($F_4 \sim \Delta^2(B_2^2 - B_1^2 B_1^2)$, $\varepsilon = 0.001$), — ($F_2 = B_2^2$, $\varepsilon = 0.001$), — ($F_2 = B_2^2$, $\varepsilon = 0.1$), - - - (Initial Packet)

accuracy in the well-resolved wavenumbers. Similarly, the second-order B-spline results demonstrate the trade-off between filtering spurious reflections in the fine resolution region and maintaining the resolved turbulence in the coarse resolution region, and how models with larger values of N perform better within the context of this trade-off.

The one-dimensional energy spectra in the fine and coarse regions are shown in Figures 10 and 11 for seventh- and second-order B-splines, respectively. The results of the model in physical space for the seventh order B-spline case with $F_{10} = \Delta^8(B_2^7 - B_1^7 B_1^7)$ and $\varepsilon = 0.001$ are shown in Figure 9. Compare these results with the pure convection case (i.e., the no model case) examined in Section 2.2. In all settings, the model makes significant corrections to the issues associated with resolution inhomogeneity. The model reduces the impact of spurious high wavenumber reflections while keeping the resolvable turbulence as intact as possible.

Figures 10a and 11a show the energy contained in the initial spurious wavenumber reflections propagating backward through the fine region. Figures 10b and 11b show the same energy propagating forward through the fine region after the secondary reflections occur when the energy is transferred back to the original fine wavenumbers. The model reduces these reflections by at least a value near ε for all choices of N . Recall

that the largest initial wavenumber with positive group velocity has the smallest reflected wavenumber and is dissipated the least by the model, so the value of ε should be validated at these wavenumbers in the energy spectra results. The dissipation levels are close to ε at this target wavenumber in all cases. All other wavenumbers are dissipated by at least ε , including both P_1 and P_2 type reflections. Moreover, in the second-order B-spline results specifically, the model constant ensures different values of N , as well as different forms of the filter, perform remarkably similar at the same level of ε in terms of reducing reflections, as desired. Overall, these results demonstrate the robustness of the model to different numerical methods, different amounts of dissipation, ε , and different numerical operators, as well as the model’s ability to correct for the issues associated with resolution inhomogeneity.

Figures 10c and 11c show the energy contained in the resolvable turbulence in the coarse resolution region. In the coarse region, the pure convection case represents the ideal spectrum as no resolvable turbulence is dissipated. The seventh-order results show how larger values of N can better preserve the resolvable turbulence while affording more dissipation in the reflections. In particular, the $B_2^7 - B_1^7 B_1^7$ model matches the ideal spectra in the coarse region almost exactly and is still able to reduce reflections by at least three orders of magnitude. Similarly, in the second-order B-spline results, the $N = 4$ cases match more closely to the original spectra than the $N = 2$ cases.

Finally, the model mitigates the effect of erroneous reflections on other incoming turbulence, as demonstrated by examining the turbulence packet after one flow through. The corresponding energy spectra are shown in Figures 10d and 11d. Even a modest reduction in the reflections — such as that from the low N and ε cases — yields much better spectra results than the pure convection case. The spectra after one flow through match quite well with the initial packet’s spectrum for all coarse wavenumbers.

4 Conclusion

Practical LES of high Reynolds number flows often dictates discretizations with highly inhomogeneous resolution. As resolved turbulence convects through a coarsening grid, the portion of the resolved turbulence that can no longer be resolved by the grid must be transferred to the subgrid scales. If filtering and differentiation commuted, the governing equations would naturally provide this additional transfer rate. However, because of the commutation error, the onus falls on the SGS model. Traditional SGS models are not equipped to produce the additional dissipation rate that is required in regions of resolution inhomogeneity because the characteristic time scale is no longer the turbulent time scale, but rather the time scale defined through the mean convection velocity, the rate of change of grid resolution, and the grid resolution itself. Moreover, this additional transfer rate can overwhelm the usual dissipation rate depending on the severity of the inhomogeneity or the strength of the convection velocity.

While the commutation error is well recognized, it is often ignored in practice because of the modeling challenges that arise. Moreover, most of the previous work on the commutation error has only applied to smooth convolution filters or has only addressed the additional commutation error that arises from applying explicit filters on top of the implicit filter. The commutation error related to the implicit filter has not been well investigated until now.

In this paper, we first uncover how the implicit commutation error manifests in simulation. It is found in Section 2 that the implicit commutation error is determined by the propagation properties of the underlying numerics. Depending on the numerics, the result can be non-physical reflected fluctuations in the fine region of the domain or non-physical transmitted fluctuations in the coarse region of the domain. This dependence on numerics makes sense as the implicit filter is defined through a projection onto the discretization. In fact, the implicit filter ensures that numerics cannot be separated from the modeling process. As Meneveau and Katz [7] mentioned in their review paper, “our understanding of the interplay between numerical and modeling issues is presently quite limited.” Several authors have sought to address this interplay and note the importance of its further investigation for robust SGS modeling [11, 42, 30, 28, 13]. The work presented here clearly highlights the inseparability of numerics and the commutation error. We emphasize the importance of considering numerical properties during the formulation of LES models, such as the group velocity, dispersion relation, and propagation properties, as in the case examined here.

The impact of the implicit commutation error is demonstrated on the energy spectrum of a packet of homogeneous isotropic turbulence convecting through an inhomogeneous grid. For the numerics considered here, scales that are not resolvable in the coarse region of the grid are reflected back into the fine region at much higher wavenumbers. Accordingly, the commutation error leads to a significant pile up of energy

in the fine region of the grid. A model is proposed for correcting the commutation error in Section 3.1 for the simple case considered here and is shown to perform well in Section 3.2. The proposed model indicates several important properties of a commutation model for LES applications, such as the inclusion of the commutation-viscosity $\nu_{comm} = a\Delta(d\Delta/dx)$ coupled with a higher order filter. Several considerations are also presented that could be applied generally to viscosity and hyperviscosity models. Particularly, we showed how numerical operators could be designed to produce higher order dissipation terms/filters without introducing higher order numerics, additional boundary conditions, or affecting CFL conditions.

Several avenues of future work were mentioned throughout the paper, which we summarize here. Now that the implicit commutation error is better understood, the commutation model should be tested on a realistic turbulent flow. To that end, we developed a statistical view of the commutation error in Section 3.1, which will be useful for further development and tuning of commutation models for turbulence applications. It will be interesting to compare instantaneous and statistical representation of the commutation error in an LES setting. The numerical properties of the implicit commutation error discovered here will also need to be extended to more complex grid settings for realistic turbulence applications. Similarly, the issue of forcing through refining grids will need to be explored. Moreover, the numerical operators developed in Section 3.1 can be used to reduce discretization error that arises even in on uniform grids. We highlight the $B_2 - B_1B_1$ operator developed in Section 3.1.1 given by the difference between the numerical second derivative operator and repeated application of the numerical first derivative operator, which acts as a filter for the insufficiently resolved scales that adapts to different numerics without needing to define ad hoc filter widths or explicit filters that introduce other errors. Overall, the insights into the implicit commutation error developed here lay a crucial foundation for addressing several deficiencies of standard SGS models, which will lead to more accurate and broadly applicable turbulence models for practical LES applications.

Appendix

A Complete Commutation Error Analysis

As in [1], any smooth nonuniform grid in the domain $a \leq x \leq b$ can be mapped to a uniform grid of spacing δ in the domain $[-\infty, \infty]$ through some monotonic differentiable mapping function $\xi = f(x)$. Using this mapping, the definition for the filtering of an arbitrary function $\psi(x)$ with a nonuniform filter width can be defined as:

$$\bar{\psi}(x) = \frac{1}{\delta} \int_a^b G\left(\frac{f(x) - f(y)}{\delta}\right) \psi(y) f'(y) dy. \quad (24)$$

Define a new variable ξ as:

$$\frac{f(y) - f(x)}{\delta} = \xi. \quad (25)$$

Equation (25) can be inverted to express y as a function of ξ in a power series about δ as

$$y = \sum_{i=0}^{\infty} \delta^i \xi^i y_i. \quad (26)$$

Using (25) and properties of formal power series, we obtain the recursive formula for y_i given $y_0 = x$, $y_1 = 1/f'(x)$:

$$y_i = - \sum_{n=2}^i \beta_{n,i-n} \frac{f^{(n)}(x)}{n! f'(x)}, \quad (27)$$

where,

$$\beta_{n,0} = y_1^n, \quad \beta_{n,m} = \frac{1}{m y_1} \sum_{k=1}^m (kn - m + k) y_{k+1} \beta_{n,m-k}. \quad (28)$$

Upon differentiation of (24) with respect to x , integration by parts, and application of (25), the commutation error, $\mathcal{C}(\psi)$, can be expressed as:

$$\mathcal{C}(\psi) \equiv \frac{d\bar{\psi}}{dx} - \frac{d\psi}{dx} = \int_{-\infty}^{\infty} G(\zeta) \psi'(y) \left[1 - \frac{f'(x)}{f'(y)} \right] d\zeta. \quad (29)$$

A general function $\phi(y)$ can be Taylor expanded about x as,

$$\phi(y) = \phi(x) + \sum_{n=1}^{\infty} \frac{\phi^{(n)}(x)}{n!} (y-x)^n. \quad (30)$$

Suppose we are interested in obtaining up to the N th order (in δ) commutation terms. Then we can express,

$$(y-x)^n = \left(\sum_{m=1}^{\infty} \delta^m \xi^m y_m \right)^n = \sum_{j=0}^{N-n} \delta^{j+n} \xi^{j+n} \beta_{n,j} + \mathcal{O}(\delta^{N+1}), \quad (31)$$

for $n > 0$. Substitution of (31) into (30) gives:

$$\phi(y) = \phi(x) + \sum_{n=1}^N \left(\frac{\phi^{(n)}(x)}{n!} \sum_{j=0}^{N-n} \delta^{j+n} \xi^{j+n} \beta_{n,j} \right) + \mathcal{O}(\delta^{N+1}). \quad (32)$$

Equation (32) can be used to expand each term in (29) about x , so that the N th order (in δ) commutation error is given by:

$$\begin{aligned} \mathcal{C}(\psi) = & \sum_{m=1}^N \left[\frac{1}{m!} \left[\psi' \left(\frac{1}{f'} \right)^{(m)} f' \right] (x) \sum_{\substack{k=0 \\ k+m \in 2\mathbb{Z}}}^{N-m} \delta^{k+m} \beta_{m,k} \int \xi^{k+m} G(\xi) d\xi \right] \\ & + \sum_{n=1}^N \sum_{m=1}^N \left[\frac{1}{n!m!} \left[\psi^{(n+1)} \left(\frac{1}{f'} \right)^{(m)} f' \right] (x) \sum_{\substack{j=0 \\ j+k+n+m \leq N \\ j+k+n+m \in 2\mathbb{Z}}}^{N-n} \sum_{k=0}^{N-m} \delta^{j+k+n+m} \beta_{n,j} \beta_{m,k} \int \xi^{j+k+n+m} G(\xi) d\xi \right] + \mathcal{O}(\delta^{N+1}) \end{aligned} \quad (33)$$

Up to second order in δ , the commutation error is given by,

$$\mathcal{C}[\psi] = \frac{2f'f''\psi'' + f'f'''\psi' - 3f''^2\psi'}{2f'^4} \delta^2 \int_{-\infty}^{\infty} \xi^2 G(\xi) d\xi + \mathcal{O}(\delta^4), \quad (34)$$

which agrees with equation (3.9) in [1].

Now, notice that (33) and (34) are expressed in terms of δ , and the unfiltered field ψ . From a modeling perspective, it would be helpful to express the commutation error in terms of the local grid spacing, Δ , and the filtered field $\bar{\psi}$. Recall, the filtering operation (24) can be written in terms of ξ as,

$$\bar{\psi}(x) = \int_{-\infty}^{\infty} G(\xi) \psi(y) d\xi. \quad (35)$$

To express the cost of replacing unfiltered terms with their abridged, yet computationally available filtered counterparts, [1] takes $\psi = \hat{\psi}_{\kappa} \exp(i\kappa x)$, substitutes this form into (35), and plugs the result back into (34) after the corresponding Taylor expansions. However, it is assumed that $\delta \ll \kappa\delta$, for all wavenumbers κ . This assumption is dimensionally inconsistent as $\delta \sim L$ and $\kappa \sim 1/L$ for some length scale L , and also invalid for small κ when considering implicit filters defined by the grid where $0 \leq \kappa\delta \leq \pi$. This assumption results in the loss of several commutation terms, which describe the impact of resolution inhomogeneity on LES.

Instead, consider the Taylor expansion of each term in (35) *directly*. Using (31) and (35), we can write:

$$\psi(x) = \bar{\psi}(x) - \sum_{n=1}^N \left(\frac{\psi^{(n)}(x)}{n!} \sum_{\substack{j=0 \\ j+n \in 2\mathbb{Z}}}^{N-n} \delta^{j+n} \beta_{n,j} \int \xi^{j+n} G(\xi) d\xi \right) + \mathcal{O}(\delta^{N+1}). \quad (36)$$

Equation (36) can be substituted back into (33) to obtain the commutation error in terms of the filtered velocity field without the loss of any terms. Moreover, the commutation error can be converted to the local

grid spacing $\Delta(x)$ using the relationship $f' = \delta\Delta^{-1}$. For the convolution filters considered [1], o second order (in δ), the complete commutation terms up to second order in δ expressed in terms of the local grid spacing and filtered velocity field are:

$$\mathcal{E}(\psi) = \left(- \left[\frac{1}{2} (\Delta'^2 + \Delta\Delta'') \right] \frac{d\bar{\psi}}{dx} - [\Delta\Delta'] \frac{d^2\bar{\psi}}{dx^2} \right) \int \zeta^2 G(\zeta) d\zeta. \quad (37)$$

Compare (37) with equation (5.9) in [1]: dispersive terms arise in addition to the dissipation term. The difference that arises when correcting for the erroneous assumption in [1] becomes more apparent when considering higher order terms. The complete fourth order terms are:

$$\begin{aligned} \mathcal{E}(\psi) = & - \left[\frac{1}{2} (\Delta'^2 + \Delta\Delta'') \right] \bar{\psi}' \int \zeta^2 G(\zeta) d\zeta - [\Delta\Delta'] \bar{\psi}'' \int \zeta^2 G(\zeta) d\zeta \\ & + \left[\frac{-\Delta'^4 - 11\Delta\Delta'^2\Delta'' - 7\Delta^2\Delta'\Delta''' - 4\Delta^2\Delta''^2 - \Delta^3\Delta''''}{24} \right] \bar{\psi}' \int \zeta^4 G(\zeta) d\zeta \\ & + \left[\frac{\Delta'^4 + 8\Delta\Delta'^2\Delta'' + \Delta^2\Delta''^2 + 2\Delta^2\Delta'\Delta'''}{4} \right] \bar{\psi}' \left(\int \zeta^2 G(\zeta) d\zeta \right)^2 \\ & + \left[\frac{-7\Delta\Delta'^3 - 13\Delta^2\Delta'\Delta'' - 2\Delta^3\Delta'''}{12} \right] \bar{\psi}'' \int \zeta^4 G(\zeta) d\zeta \\ & + \left[\frac{11\Delta\Delta'^3 + 11\Delta^2\Delta'\Delta''}{4} \right] \bar{\psi}'' \left(\int \zeta^2 G(\zeta) d\zeta \right)^2 \\ & + \left[\frac{-3\Delta^2\Delta'^2 - \Delta^3\Delta''}{4} \right] \bar{\psi}''' \int \zeta^4 G(\zeta) d\zeta + \left[\frac{11\Delta^2\Delta'^2 + \Delta^3\Delta''}{4} \right] \bar{\psi}''' \left(\int \zeta^2 G(\zeta) d\zeta \right)^2 \\ & + \left[\frac{-\Delta^3\Delta'}{6} \right] \bar{\psi}'''' \int \zeta^4 G(\zeta) d\zeta + \left[\frac{\Delta^3\Delta'}{2} \right] \bar{\psi}'''' \left(\int \zeta^2 G(\zeta) d\zeta \right)^2 \end{aligned} \quad (38)$$

The original analysis in [1] would only include the second term and last two terms in (38).

Equations (33) and (36) can *easily* be computed using a symbolic manipulation tool to generate terms of the commutation error. However, the expressions are quite complex, and the analysis is not applicable to implicit filters anyways. As shown in section 3.1, it will be more useful from a modeling approach if we can gain an understanding of the general *structure* of commutation error. To that end, notice that, up to a constant, the values of y_i in (27) scale like:

$$y_i \sim \left[\frac{d^{i-1}}{dx^{i-1}} \left(\frac{1}{f'} \right) \right] \left(\frac{1}{f'} \right)^{i-1} \quad (39)$$

Propagating this into the definition of the commutation error, and noticing that the procedure given by equation (36) will not change the form of the commutation error, gives:

$$\mathcal{E}(\psi) \sim \sum_{N=1}^{\infty} \delta^{2N} \sum_{i=1}^{2N} \frac{\partial^i \bar{\psi}}{\partial x^i}(x) \left[\frac{d^{2N-i+1}}{dx^{2N-i+1}} \left(\frac{1}{f'} \right) \right] \left(\frac{1}{f'} \right)^{2N-1}. \quad (40)$$

Expressing (40) in terms of the local grid spacing gives the general form of the N th order commutation error:

$$\mathcal{E}(\psi) = \sum_{n=1}^{N/2} \sum_{m=1}^{2n} C_{mn} \Delta^{2n-m} \left[\frac{\partial^{2n-m+1} \bar{\psi}}{\partial x^{2n-m+1}} \right] \frac{d^m \Delta^m}{dx^m} + \mathcal{O}(\delta^{N+2}), \quad (41)$$

for even N . As before, the constants C_{mn} formally depend on the moments of the filter, which suggests the constants should dependent on the underlying discretization for an implicitly filtered LES.

B Commutation Model Coefficient

Let ε be a tolerance level indicating the desired amount of reduction in the energy in reflections, e.g., $\varepsilon = 0.1$ implies *at least* a factor of ten reduction in the reflected energy for all wavenumbers. We can get an intuition

for the desired coefficient by considering the following equation:

$$\frac{\partial \hat{u}(\kappa, t)}{\partial t} = (-1)^{\frac{N-2}{2}} Ca \frac{\partial \Delta}{\partial x} \Delta^{N-1} \hat{F}_N(\kappa) \hat{u}(\kappa, t), \quad (42)$$

where a is the convective velocity, and $\hat{F}_N(\kappa)$ represents the value of the spectrum of the F_N operator for wavenumber κ , i.e., $\hat{F}_N(\kappa) \approx (i\kappa)^N$. After time t , the amplification felt by a given wavenumber κ is:

$$\hat{u}(\kappa, t) = \hat{u}(\kappa, 0) \exp \left((-1)^{\frac{N-2}{2}} Ca \frac{\partial \Delta}{\partial x} \Delta^{N-1} \hat{F}_N(\kappa) t \right). \quad (43)$$

We desire $\hat{u}^2(\kappa, t)/\hat{u}^2(\kappa, 0) \leq \epsilon$ for all scales approaching unresolvability. Solving for the constant C gives,

$$C \geq \frac{(-1)^{\frac{N-2}{2}} \log(\epsilon)}{2a \frac{\partial \Delta}{\partial x} \Delta^{N-1} \hat{F}_N(\kappa) t}. \quad (44)$$

If we assume that $d\Delta/dx \approx (\max(\Delta) - \min(\Delta))/L_\Delta$ and that the time a reflection feels the dissipation is $t = L_\Delta/(ga)$, for some length of gradual coarsening L_Δ and group velocity factor g , the (44) simplifies to

$$C \geq \frac{(-1)^{\frac{N-2}{2}} \log(\epsilon)}{\frac{2}{g} \left(\frac{\max(\Delta) - \min(\Delta)}{\Delta} \right) \left(\Delta^N \hat{F}_N(\kappa) \right)}. \quad (45)$$

The assumptions on $d\Delta'/dx$ and t are reasonable: if the resolution change is abrupt, the strength of the dissipation will be greater, but the amount of time the dissipation is felt will be less. In contrast, if the change in resolution is gradual, the dissipation will be weaker, but it will be felt longer. Therefore, we postulate that only the absolute change in resolution over a certain length should affect the constant. Moreover, for simplicity we assume the group velocity is on average twice as fast as the convection velocity for the reflected wavenumbers considered in section 2.2.1, and take $g = 2$. This is based on the maximum and minimum group velocity for second and seventh order B-splines but could be further tuned according to the numerics to yield better results.

Lastly, we take $\kappa \equiv \kappa_a$ (as explain in section 3.1.2) and the isolated $\Delta \equiv \max(\Delta)$ to maintain a lower bound. With these assumptions, the constant is given by:

$$C = \frac{(-1)^{\frac{N-2}{2}} \log(\epsilon)}{\left(\frac{\max(\Delta) - \min(\Delta)}{\max(\Delta)} \right) \left(\Delta^N \hat{F}_N(\kappa_a) \right)}. \quad (46)$$

Acknowledgments

The authors acknowledge the generous financial support from the National Aeronautics and Space Administration (cooperative agreement number NNX15AU40A), the National Science Foundation (project number 1904826), and the U.S. Department of Energy, Exascale Computing Project (subcontract number XFC-7-70022-01 from contract number DE-AC36-08GO28308 with the National Renewable Energy Laboratory). Thanks are also due the Texas Advanced Computing Center at The University of Texas at Austin for providing HPC resources that have contributed to the research results reported here.

References

- [1] Sandip Ghosal and Parviz Moin. The basic equations for the large eddy simulation of turbulent flows in complex geometry. *Journal of Computational physics*, 118(1):24–37, 1995.
- [2] Harmen van der Ven. A family of large eddy simulation (les) filters with nonuniform filter widths. *Physics of Fluids*, 7(5):1171–1172, 1995.
- [3] Oleg V Vasilyev, Thomas S Lund, and Parviz Moin. A general class of commutative filters for les in complex geometries. *Journal of computational physics*, 146(1):82–104, 1998.

- [4] Alison L Marsden, Oleg V Vasilyev, and Parviz Moin. Construction of commutative filters for les on unstructured meshes. *Journal of Computational Physics*, 175(2):584–603, 2002.
- [5] Michele Iovieno and Daniela Tordella. Variable scale filtered navier–stokes equations: a new procedure to deal with the associated commutation error. *Physics of Fluids*, 15(7):1926–1936, 2003.
- [6] Pierre Sagaut. *Large eddy simulation for incompressible flows: an introduction*. Springer Science & Business Media, 2006.
- [7] Charles Meneveau and Joseph Katz. Scale-invariance and turbulence models for large-eddy simulation. *Annual Review of Fluid Mechanics*, 32(1):1–32, 2000.
- [8] Sharath S Girimaji and Stefan Wallin. Closure modeling in bridging regions of variable-resolution (vr) turbulence computations. *Journal of Turbulence*, 14(1):72–98, 2013.
- [9] Sigfried William Haering et al. *Anisotropic hybrid turbulence modeling with specific application to the simulation of pulse-actuated dynamic stall control*. PhD thesis, 2015.
- [10] TS Lund. The use of explicit filters in large eddy simulation. *Computers & Mathematics with Applications*, 46(4):603–616, 2003.
- [11] C Fureby and G Tabor. Mathematical and physical constraints on large-eddy simulations. *Theoretical and Computational Fluid Dynamics*, 9(2):85–102, 1997.
- [12] Fujihito Hamba. Analysis of filtered navier–stokes equation for hybrid rans/les simulation. *Physics of Fluids*, 23(1):015108, 2011.
- [13] Sandip Ghosal. An analysis of numerical errors in large-eddy simulations of turbulence. *Journal of Computational Physics*, 125(1):187–206, 1996.
- [14] Fotini Katopodes Chow and Parviz Moin. A further study of numerical errors in large-eddy simulations. *Journal of Computational Physics*, 184(2):366–380, 2003.
- [15] AG Kravchenko and Parviz Moin. On the effect of numerical errors in large eddy simulations of turbulent flows. *Journal of computational physics*, 131(2):310–322, 1997.
- [16] Daniele Carati, Grégoire S Winckelmans, and Hervé Jeanmart. On the modelling of the subgrid-scale and filtered-scale stress tensors in large-eddy simulation. *Journal of Fluid Mechanics*, 441:119–138, 2001.
- [17] Jessica Gullbrand and Fotini Katopodes Chow. The effect of numerical errors and turbulence models in large-eddy simulations of channel flow, with and without explicit filtering. *Journal of Fluid Mechanics*, 495:323–341, 2003.
- [18] Andrew W Cook and William H Cabot. Hyperviscosity for shock-turbulence interactions. *Journal of Computational Physics*, 203(2):379–385, 2005.
- [19] Lloyd N Trefethen. Group velocity in finite difference schemes. *SIAM review*, 24(2):113–136, 1982.
- [20] Robert Vichnevetsky. Energy and group velocity in semi discretizations of hyperbolic equations. *Mathematics and Computers in Simulation*, 23(4):333–343, 1981.
- [21] Robert Vichnevetsky. Group velocity and reflection phenomena in numerical approximations of hyperbolic equations. *Journal of the Franklin Institute*, 315(5-6):307–330, 1983.
- [22] Robert Vichnevetsky. Propagation through numerical mesh refinement for hyperbolic equations. *Mathematics and Computers in Simulation*, 23(4):344–353, 1981.
- [23] David Long and John Thuburn. Numerical wave propagation on non-uniform one-dimensional staggered grids. *Journal of Computational Physics*, 230(7):2643–2659, 2011.

- [24] Robert Vichnevetsky. Wave propagation and reflection in irregular grids for hyperbolic equations. *Applied Numerical Mathematics*, 3:133–166, 1987.
- [25] J Frank and S Reich. On spurious reflections, nonuniform grids and finite difference discretizations of wave equations. cwi report mas-e0406. *Center for Mathematics and Computer Science*, 2004.
- [26] Uri M Ascher and Robert I McLachlan. Multisymplectic box schemes and the korteweg–de vries equation. *Applied Numerical Mathematics*, 48(3-4):255–269, 2004.
- [27] Christer Fureby and Fernando F Grinstein. Large eddy simulation of high-reynolds-number free and wall-bounded flows. *Journal of Computational Physics*, 181(1):68–97, 2002.
- [28] Fernando F Grinstein, Len G Margolin, and William J Rider. *Implicit large eddy simulation: computing turbulent fluid dynamics*. Cambridge university press, 2007.
- [29] Alexander N Brooks and Thomas JR Hughes. Streamline upwind/petrov-galerkin formulations for convection dominated flows with particular emphasis on the incompressible navier-stokes equations. *Computer methods in applied mechanics and engineering*, 32(1-3):199–259, 1982.
- [30] Y Bazilevs, VM Calo, JA Cottrell, TJR Hughes, A Reali, and G Scovazzi. Variational multiscale residual-based turbulence modeling for large eddy simulation of incompressible flows. *Computer methods in applied mechanics and engineering*, 197(1-4):173–201, 2007.
- [31] A Kravchenko, Parviz Moin, Karim Shariff, A Kravchenko, P Moin, and K Shariff. B-spline method and zonal grids for simulations of complex turbulent flows. In *35th Aerospace Sciences Meeting and Exhibit*, page 433, 1999.
- [32] Karim Shariff and Robert D Moser. Two-dimensional mesh embedding for b-spline methods. *Journal of Computational Physics*, 145(2):471–488, 1998.
- [33] Wai Yip Kwok, Robert D Moser, and Javier Jiménez. A critical evaluation of the resolution properties of b-spline and compact finite difference methods. *Journal of Computational Physics*, 174(2):510–551, 2001.
- [34] Myoungkyu Lee and Robert D Moser. Direct numerical simulation of turbulent channel flow up to $re_\tau \approx 5200$. *Journal of Fluid Mechanics*, 774:395–415, 2015.
- [35] Philippe R Spalart, Robert D Moser, and Michael M Rogers. Spectral methods for the navier-stokes equations with one infinite and two periodic directions. *Journal of Computational Physics*, 96(2):297–324, 1991.
- [36] Robert Vichnevetsky. Wave propagation analysis of difference schemes for hyperbolic equations: a review. *International Journal for Numerical Methods in Fluids*, 7(5):409–452, 1987.
- [37] Jean-Pierre Berenger. A perfectly matched layer for the absorption of electromagnetic waves. *Journal of computational physics*, 114(2):185–200, 1994.
- [38] Robert Vichnevetsky and Thomas Scheidegger. The nonlocal nature of internal reflection in computational fluid dynamics with spectral methods. *Applied numerical mathematics*, 8(6):533–539, 1991.
- [39] C David Pruett, James S Sochacki, and Nikolaus A Adams. On taylor-series expansions of residual stress. *Physics of Fluids*, 13(9):2578–2589, 2001.
- [40] JA Domaradzki and Nikolaus A Adams. Direct modelling of subgrid scales of turbulence in large eddy simulations. *Journal of Turbulence*, 3(024):1, 2002.
- [41] Jorge Bardina, J Ferziger, and W Reynolds. Improved subgrid-scale models for large-eddy simulation. In *13th fluid and plasmadynamics conference*, page 1357, 1980.
- [42] Thomas JR Hughes, Luca Mazzei, and Kenneth E Jansen. Large eddy simulation and the variational multiscale method. *Computing and visualization in science*, 3(1-2):47–59, 2000.